Intracellular dsRNA induces apoptotic cell death via the synergistic activation of PKR and TLR3

Zuo Wenjie

Table of contents   Page

ABSTRACT

RIG-I like receptors (RLRs), protein kinase R (PKR), and endosomal Toll-like receptor 3 (TLR3) are essential pattern recognition receptors for sensing viral non-self RNA and are involved in the determination of cell fate. Both RLRs and TLR3 are powerful engines for the induction of interferon, and PKR on the other hand, serves to regulate cellular stress in response to danger signals. Viruses accumulate RNA species with different features at intra- and extra-cellular space, and the actions of multiple RNA receptors are simultaneously induced during viral infection. Thereby, a resulted cellular event, such as apoptosis, is believed to be executed via cooperative signaling. However, the mechanisms by which intracellular RNA induces apoptosis, particularly the role of each RNA sensor, remain uninvestigated.

In this study, cytoplasmic injections of different RNA were performed at single cell level and followed by live cell imaging to elucidate the molecular mechanisms underlying viral dsRNA-induced apoptosis. The obtained results revealed that short dsRNA with 5′-triphosphate, the sole ligand of RIG-I, induced slow apoptosis in a small portion of cells depending on the IRF-3 transcriptional activity and the production of IFN-I. However, cytoplasmic long dsRNA, which could be sensed by multiple RNA receptors, was confirmed to trigger distinct signals, and synergistically induce drastic apoptosis via PKR and TLR3. RLRs, on the other hand, was shown to play minor role in this cell death synergy. PKR activation resulted in the arrest of translational machinery and markedly reduced the level of cellular FLICE-like inhibitory protein (cFLIP) which functioned in the TLR3/TRIF-dependent activation of caspase 8. cFLIP, as a short-life inhibitor of caspase 8, exhibited its significance in cell death determination during the cooperative signaling triggered by cytoplasmic dsRNA.

The present study demonstrated that PKR and TLR3 were both important for inducing the viral RNA-mediated apoptosis and the resulted inhibition of viral production in infected cells.

ABBREVIATIONS

5'-ppp	5 end triphosphate
ADAR1	Adenosine deaminase acting on RNA
AIM2	Absent in melanoma 2
Bak	Bcl-2 antagonist/killer 1
Bax	Bcl-2-associated X protein
Bcl-2	B-cell lymphoma 2
CARD	Caspase activation and recruitment domain
cFLIP L	Cellular FLICE like inhibitory protein long isoform
cFLIP S	Cellular FLICE like inhibitory protein short isoform
cGAS	Cyclic GMP–AMP synthase
CHX	Cycloheximide
CTD	Carboxy terminal domain
CBP	Cyclic adenosine monophosphate response element binding protein
DISC	Death inducing signaling complex
dsRNA	Double stranded RNA
ssRNA	Single stranded RNA
eIF2α	Eukaryotic initiation factor 2 α
FADD	Fas-associated protein with death domain
FAS	Fas cell surface death receptor
G3BP1	Ras GTPase-activating protein-binding protein 1
GCN2	General control nonderepressible 2
GFP	Green fluorescent protein
GSDMD	Gasdermin D
GyrB	DNA gyrase subunit B
HRI	Heme-regulated eIF2α kinase
IFN-I	Type I interferon
IFNAR1	Interferon alpha and beta receptor subunit 1
IFN-β	Interferon β
IKKβ	Inhibitor of nuclear factor kappa B kinase subunit β
IL-1β	Interleukin 1 β
IPS-1	Interferon promoter stimulator-1
IRF-3	Interferon regulatory factor 3
ISG	Interferon stimulated gene
JAK	Janus kinase
LGP2	Laboratory of genetics and physiology 2
MAPK	Mitogen-activated protein kinase
MDA5	Melanoma differentiation-associated protein 5
MLKL	Mixed lineage kinase domain-like protein
Myd88	Myeloid differentiation primary response 88
Nf-kB	Nuclear factor kappa B
NLRP3	NLR family pyrin domain containing 3
OAS1	2'-5'-Oligoadenylate synthetase 1

P300	Histone acetyltransferase p300
PACT	Protein activator of protein kinase R
PAMPs	Pathogen-associated molecular patterns
PERK	Protein kinase R-like endoplasmic reticulum kinase
PARP	Poly (ADP-ribose) polymerase
PKR	Protein kinase activated by RNA
Poly I:C	Polyinosinic:polycytidylic acid
PRRs	Pattern recognition receptors
RIG-I	Retinoic acid-inducible gene I
RIPK3	Receptor interacting serine/threonine kinase 3
RLRs	RIG-I like receptors
SeV	Sendai virus
SG	Stress granule
SINV	Sindbis virus
STAT	Signal transducer and activator of transcription
TBK1	Tank binding kinase 1
TIAR	TIA1 cytotoxic granule associated RNA binding protein like 1
TLRs	Toll like receptors
TNFα	Tumor necrosis factor α
TRAIL	TNF-related apoptosis-inducing ligand
TRIF	TIR-domain-containing adapter-inducing interferon-β

CHAPTER 1

INTRODUCTION

1.1   Overview of innate immunity

Innate immunity is human's first line of defense against foreign pathogens such as viruses, bacteria, fungi and parasites. Innate immunity senses the foreign danger signals by recognizing their pathogen associated molecular patterns (PAMPs) via the cellular pathogen recognition receptors (PRRs). These receptors activate subsequential signals which lead to the expression of various genes to achieve the inhibition and elimination of pathogenic materials. The process of innate immunity against viral infection involves a variety of cells and actions. Epithelial and endothelial cells are usually the first cells to be exposed to viral particles, the natural killing cells, macrophages, neutrophils and dendritic cells participate in the virus clearance and amplification of immune signals in the host. These actions further stimulate adaptive immunity and recruits T cells and B cells to perform cellular or humoral immunity respectively. The response of innate immunity is rapid, and the secretion of interferon and critical cytokines can usually be achieved within a few hours after infection. The prompt activation of innate immunity served to control the viral replication, and protect host cells from further damage (Akira et al., 2001; Janeway & Medzhitov, 2002).

My research focuses on the recognition and inhibition of viruses by the innate immune system. During viral infection, viruses inject their genetic material, DNA or RNA, into cells, relying on the host cell environment, they complete replication, transcription, translation and release of matured viral particles to further infect surrounding cells. Viral nucleic acids were recognized by PPRs in host cells due to their structural peculiarities. There are various type of PPRs in human cells responsible for recognizing and processing the signaling of foreign DNA and RNA, for instance, TLRs, RLRs, PKR, etc., which will be covered one by one below.

1.2   Toll like receptors (TLRs)

TLR family has many members, TLR1/2/3/4/5/6/7/8/9/10 have been found expressing in human cells. Among which, TLR3/7/8 exist in the endosome and are important recognition receptors for extracellular RNA, TLR7/8 recognize GU rich ssRNA, TLR3 recognize dsRNA. RNA viruses produce large amounts of dsRNA during replication in host cells; moreover, these dsRNA when released extracellularly can re-enter the cells through

endocytosis and be recognized by the endosomal TLR3. Different TLRs make use of different TIR domain-containing adaptor proteins to activate downstream signaling. Most TLRs, including TLR7/8, signal through Myd88 to trigger the activation of NF-kB, MAPKs and IRF-3, in contrast, TLR3/4 utilize TRIF to complete this step (Kawai & Akira, 2010). Later IKKβ dependent TBK1 phosphorylation further stimulate TRIF phosphorylation which promoted the recruitment of essential transcriptional factors such as IRF-3 (Abe et al., 2020; Fitzgerald et al., 2003). The activation of IRF-3 will then induce the secretion of interferon and various cytokines.

1.3 Cytoplasmic RIG-I like receptors (RLRs)

Cells also possess intracellular RNA receptors, such as RLRs to sense cytoplasmic content of non-self RNA (Kato et al., 2006; Satoh et al., 2010; Yoneyama et al., 2004). The RLR family has three members, RIG-I, MDA5 and LGP2, of which RIG-I and MDA5 are structurally similar, both consisting of a CTD and a Helicase domain for RNA binding, and two CARD domains for signaling transduction. In contrast, LGP2 is unable to participate in the signaling process due to the absence of the CARD domain. (Yoneyama et al., 2005) RIG-I specifically recognizes short-stranded dsRNA with 5'-ppp. mRNAs synthesized in the human body are generally modified by capping to avoid the formation of 5'-ppp, therefore, RNA fragments with 5'-ppp are treated as non-self RNA by RIG-I and activate the immune response (Hornung et al., 2006; Pichlmair et al., 2006). RIG-I has a relatively self-restricted structure, and its overexpression does not induce its activation. A conformational change is required for RIG-I after binding with 5'-ppp-dsRNA to release the CARD domain for interacting with mitochondrial adaptor protein IPS-1 (Kawai et al., 2005; Takahasi et al., 2008; Yoneyama & Fujita, 2008). In contrast, MDA5 senses long dsRNA (Kato et al., 2008) and was believed to have a more opened structure for its CARD, with overexpression, it can directly activate the downstream signaling cascades for IFN-I induction. IPS-1 also known as MAVS, VISA and Cardif is an essential protein embedded in the mitochondrial outer membrane for interferon stimulation. In response to the signals from the CARD of RIG-I and MDA5, mitochondrial IPS-1 forms aggregates (Hou et al., 2011a), which further transmit signals to TBK1 and IKKβ to recruit transcription factors

IRF-3/7 and Nf-kB for inducing interferon production (Kato et al., 2006; Kawai et al., 2005; Seth et al., 2005). Recent study shown that LGP2 assists in the MDA5 filamentation step by catalyzing ATP hydrolysis, which is essential for MDA5 signaling (Duic et al., 2020). Gain of function mutants of RLRs resulted in the sustained activation of the immune system leading to a variety of inflammatory and autoimmune disorders (Kato et al., 2017), therefore, understanding the mechanism and the consequence of RLRs activation are pivotal for tackling the innate immune diseases.

1.4   Protein kinase activated by RNA

Moreover, the intracellular dsRNA receptor PKR also plays an important role in the antiviral process. PKR can bind intracellular dsRNA larger than 30 bps and is also a highly elevated ISG upon the influence of interferon. However, unlike TLRs and RLRs, activation of PKR does not directly stimulate interferon production, on the other hand, it acts as a stress mediator that controls cellular homeostasis. Upon binding with dsRNA, PKR undergoes dimerization and phosphorylation which subsequently induce phosphorylation of eIF2α and resulting in *de novo* protein synthesis shut down (Samuel, 1993). This action is crucial for inhibiting viral protein expression (García et al., 2007; Lemaire et al., 2008). PKR can also be activated by PACT proteins, chemical compounds (arsenite), and a variety of cellular stress signals, (heat-shock, UV, etc.) to trigger strong apoptotic signals (Gal-Ben-Ari et al., 2018; Gil et al., 2002; Gil & Esteban, 2000; Jagus et al., 1999; Yeung et al., 1996). It has been shown that dsRNA-induced activation of PKR can trigger the formation of stress granule (SG), a cytoplasmic spot where intracellular viral nucleic acids and their receptors are gathered. RLRs and cytosolic DNA sensor cGAS have been reported to be recruited to SG, and this process greatly contribute to the induction of interferon (Hu et al., 2019; Onomoto et al., 2012). Stress responses deliver critical information to the cell compartments and mediate cellular events such as apoptosis, however the role of PKR in assisting other RNA-induced signaling remained unelucidated. The high expression of PKR in response to interferon also makes it of interest in neurodegenerative diseases, inflammatory diseases, and human metabolism (Gal-Ben-Ari et al., 2018).

Besides the above receptors, ADAR1, NLRP3, OAS1 were also shown to bind with

cytosolic dsRNA and mediate innate immune responses (Donovan et al., 2013; Franchi et al., 2014; Han et al., 2014; Liddicoat et al., 2015; Swanson et al., 2019). Moreover, other receptors like cGAS, AIM2 were reported as critical compartments for the sensing of cytosolic DNA fragments (Bürckstümmer et al., 2009; Sun et al., 2013).

1.5 IRF-3 activation and IFN-β production

IRF-3 is an important transcription factor belongs to the IRF family that induces interferon production during viral infection. IRF-3 is naturally distributed in the cytoplasm but exhibits the nuclear localization upon activation. This action is initiated by the upstream signals from RLR-IPS-1, or TLR-TRIF/Myd88 (Medzhitov et al., 1998; Oshiumi et al., 2003; Seth et al., 2005; Yamamoto et al., 2003) . Through the TBK1/IKKβ dependent phosphorylation, IRF-3 translocates into nucleus and binds with IFN-I promoter with the help of p300 and CBP, thus inducing IFN-I production. Various functions of IRF-3 including nuclear import/export and DNA binding are critical for the induction of IFN-I (Yoneyama et al., 1998).

When the secreted interferon is recognized by the interferon receptor located on the cell membrane, it activates the JAK-STAT pathway, and in turns, induces the production of various ISGs (Renauld, 2003). Expression of ISGs, throughout, promotes viral recognition and elimination. Interferon mediated positive feedback loop of immune signaling is a critical step for human body to fight against viral infection (Illustration. 1). Viruses have developed multiple mechanisms to block interferon production that dampens host immune responses and causes severe infection symptoms. However, excessive secretion of interferon may create cytokine storms that disrupt cellular homeostasis and eventually cause the inflammatory and autoimmune diseases (Kawai & Akira, 2006. The regulation of interferon has been widely studied for decades which greatly contributed to the improvement of human disease treatments.
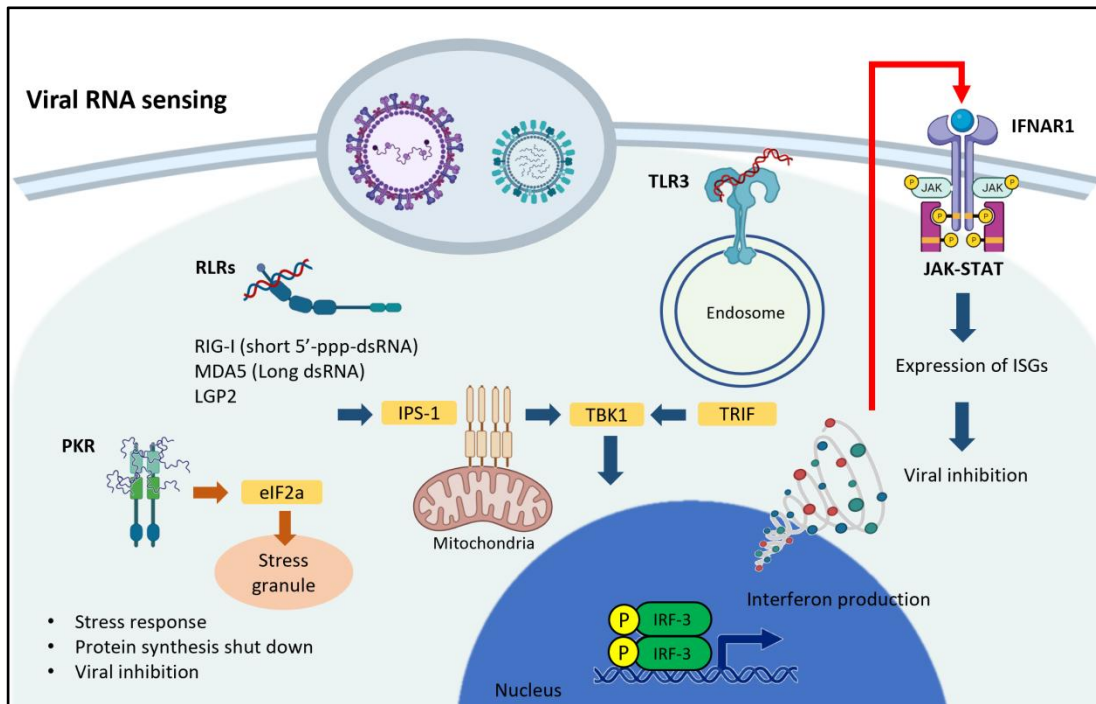
(Illustration. 1 Viral RNA sensing)

1.6 Programed cell death and their roles in innate immunity

Cell death is commonly induced during viral infections. It can be classified into "programmed death", a regulated type of cell death by internal cellular mechanisms, and "cell necrosis", an unregulated type of cell death caused by external factors such as extreme temperature, UV, toxins, physical perforation etc. Programmed cell death includes apoptosis, necroptosis, pyroptosis and ferroptosis, and their activation differs by mechanisms. Apoptosis is the most common form of programmed cell death and is manifested by the activation of multiple caspases and the formation of apoptotic bubbles (Elmore, 2007). Necroptosis, with appearance similar to necrosis, is activated by MLKL and RIPK3 in the absence of caspase 8, which is usually triggered by TLR ligands and TNFα (Vandenabeele et al., 2010). Pyroptosis is a lytic cell death, caused by severe infection cases in a highly inflammatory form, it is triggered by the activation of caspase 1 and the release of GSDMD (Bergsbaken et al., 2009). This process releases large amounts of inflammatory cytokines such as IL-1β. Ferroptosis is a recently discovered mode of programmed cell death, which is usually caused by iron accumulation and lipid peroxidation in a caspase-independent manner (Li et al., 2020). Programmed cell death plays indispensable role in antiviral immunity. As a species that depends on host cells for survival, viruses fully utilize cellular

resources for self-replication. When viral replication is matured, cells will be ruptured, and viral particles will be released to the surrounding environment for further infection. Programmed cell death essentially disrupted the environment required for viral survival. Moreover, apoptosis encapsulated the intracellular material within the apoptotic bubbles which will be cleaned up by the phagocytosis. This process not only reduces the concentration of viral particles, but also attenuates the inflammatory response caused by the release of additional cytokines.

1.7 Mechanisms underlying apoptosis activation

In contrast to cytokine production, apoptosis is executed carefully by the integrated cellular responses. The pathways that trigger apoptosis can be broadly divided into two categories, the intrinsic and the extrinsic (Illustration. 2). The former is mainly regulated by the actions of mitochondria through the release of cytochrome C and the activation of caspases 3/7/9. The latter extrinsic pathway is activated by extracellular factors like TNFα, TRAIL and Fas, etc. These actions recruit FADD/RIPK1 and form a DISC to promote the oligomerization and proteolytic cleavage of caspase 8 (Elmore, 2007). Inhibitors of caspase 8 are important regulators of extrinsic apoptosis and act as switches between apoptosis and necroptosis (Fritsch et al., 2019; Tsuchiya et al., 2015). cFLIP is an endogenous caspase 8 homolog that serves as a caspase 8 inhibitor, it expresses L and S isoform in human cells, and both of which bind to caspase 8 to form heterodimers. cFLIP L/S have shown different regulatory functions on the activation of pro-caspase 8 (Geserick et al., 2008; Safa, 2012; Tsuchiya et al., 2015). The expression of cFLIP differs with cell types, and it is commonly expressed in cancer cells at a high level to inhibit apoptosis (Alkurdi et al., 2018).

During viral infection, apoptotic signaling can be initiated by diverse nucleic acid receptors and adaptor proteins. Specific to RNA viruses, it has been shown that IPS-1 activation leads to the induction of mitochondrial inner membrane potential, resulting in the activation of Bcl-2 family protein Bak and Bax, and the release of cytochrome C (Lei et al., 2009). In addition, PKR was also reported to activate apoptosis by interacting with both mitochondria (García et al., 2007; Gil et al., 2002) and caspase 8 (García et al., n.d., 2007; Gil & Esteban, 2000; Hsu et al., 2004; Jagus et al., 1999; Yeung et al., 1996) . TLR3 can also induce

extrinsic apoptosis by activating TRIF-FADD-Caspase 8 DISC in reported cells (Alkurdi et al., 2018; McAllister et al., 2013; Salaun et al., 2006). Recent findings suggested that IRF-3 is involved in the regulation of apoptosis by activating the mitochondrial pathway through ubiquitination and mitochondrial translocation (Chattopadhyay et al., 2016; Raja & Sen, 2021) . Moreover, RIG-I was shown to activate apoptosis through OAS1 and RNase L (Boehmer et al., 2021). Finally, interferon production is also believed to play an important regulatory role in apoptosis as it upregulates essential ISGs, including RIG-I, PKR, OAS1, etc., which function in the RNA induced signaling. However, the mechanisms underlying apoptosis induced by viral RNA required further exploration. The activation of individual RNA receptor and how these signals contribute to the cell death determination needs to be thoroughly investigated.
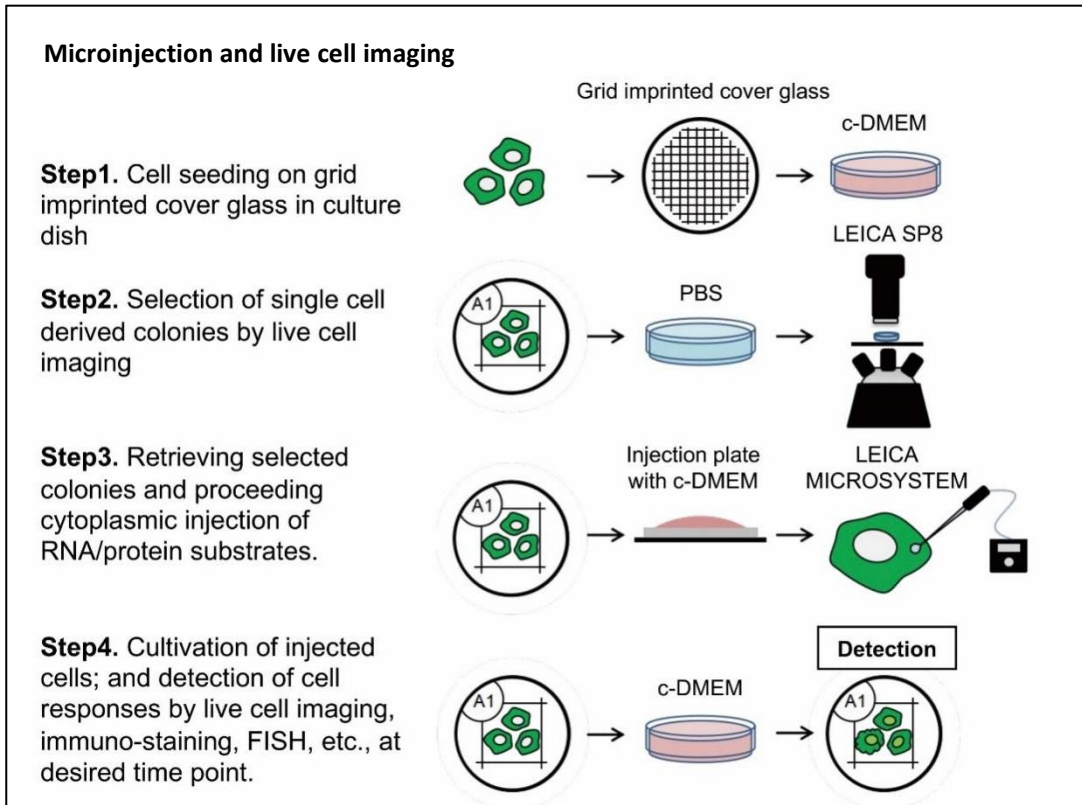
Viral RNA mimics were often used to examine the signaling pathways that RNA viruses activate. However, different RNA mimics induce distinct cellular responses as they were delivered to cells by different methods. Poly I:C, as a commonly used dsRNA mimics, activates endosomal TLR3 when exogenously treated in cell culture medium. To activate cytosolic dsRNA sensor such as RLRs, poly I:C and 5'-ppp-RNA must be transfected with the assist of lipofectamine. Both ways are commonly used to stimulate IFN-I secretion, however, the induction of apoptosis and production of IFN-I do not necessarily coincide, suggesting that they are governed by distinct mechanisms. In tumor cells, the cytoplasmic poly I:C has been shown to substantially trigger apoptosis through unidentified pathways. However what role does 5'-ppp-RNA play in the apoptosis induction still remains undiscovered.
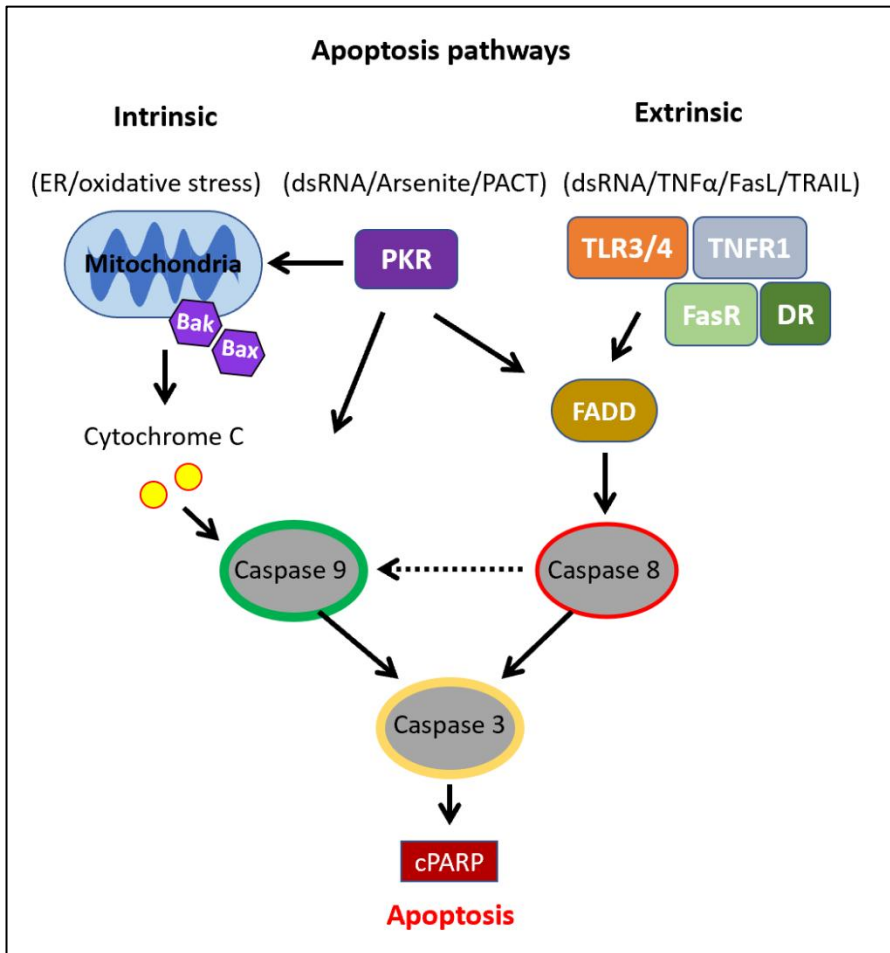
(Illustration. 2 Apoptosis pathways)

1.8   Microinjection and utilization

In this study, we utilized microinjection to deliver viral RNA mimics to cell cytoplasm, this method induced prompt and potent cellular responses (Illustration. 3). Compared to lipofectamine based transfection, microinjection significantly reduced the amount of extracellular RNA in the culture medium, and with no concerns of transfection efficiency. Along with a live cell imaging system, responses of single cells to the stimulus of the injected substrates can be easily visualized, such as the translocation of IRF-3 and the morphological alteration of cells. The use of microinjection has become popular in recent years, in areas such as transgenic mouse modeling, germline cell construction and in-vitro fertilization. And more attentions have been drawn for its potential application in the drug delivering (Moody, 2018; Tiefenboeck et al., 2018; Xu, 2019).

Microinjection and live cell imaging

Grid imprinted cover glass

c-DMEM

Step1. Cell seeding on grid imprinted cover glass in culture dish

LEICA SP8

Step2. Selection of single cell derived colonies by live cell imaging

PBS

Step3. Retrieving selected colonies and proceeding cytoplasmic injection of RNA/protein substrates.

Injection plate with c-DMEM

LEICA MICROSYSTEM

Step4. Cultivation of injected cells; and detection of cell responses by live cell imaging, immuno-staining, FISH, etc., at desired time point.

c-DMEM

Detection

(Illustration. 3 Microinjection and live cell imaging)

1.9 Purpose of the study

The current investigation focused on the role of RLRs, TLR3, and PKR in the mechanisms underlying dsRNA-induced cell death. I delivered RNA and protein into the cell cytoplasm by using microinjection and tracked the progression of cellular events within single cells. To clarify the specific functions that critical signaling components played in the programmed cell death, we created knockout (KO) cell lines for these components. The following study demonstrated that cytosolic 5'-ppp-RNA-induced apoptosis was a result of IFN-I production, however, dsRNA-induced apoptosis required the cooperation of two receptors PKR and TLR3, one located in the cytoplasm and one in the endosome. And I discovered that PKR mediated down-regulation of caspase 8 inhibitor cFLIP essentially promoted TLR3-dependent apoptotic signaling in HeLa cells. The current findings further imply that, in addition to the direct antiviral effect contributed by IFN-I, apoptosis induced by viral RNA is a host mechanism that restricts viral reproduction as well.

CHAPTER 2

MATERIALS AND METHODS

2.1 Cells and plasmids

Wild-type HeLa cells (#CCL-2.2, ATCC) and derivatives were grown in c-DMEM containing high glucose DMEM (Nacalai Tesque) + 5% Fetal Bovine Serum (FBS, Gibco) + 1% Penicillin-Streptomycin (P/S Nacalai Tesque) at 37°C in a 5% CO_2 incubator. To prevent mycoplasma contamination cells were routinely treated with plasmocin (InvivoGen). HeLa cells with RIG-I, MDA5, IPS-1, IRF-3, IFNAR1, PKR, TRIF single KO and TRIF PKR double KO (DKO) were generated using CRISPR-cas9 method, the backbone plasmid pSpCas9(BB)-2A-GFP (PX458) was kindly provided by Dr. Feng Zhang (Addgene plasmid #48138). Cells transiently transfected (48 h) with CRISPR-cas9 plasmid were sorted by GFP using SH800S Cell Sorter (SONY) and subjected to single-cell clone selection in 98-well plate. The sequences of single guide RNA (sgRNA) for each target were shown below:

RIG-I sgRNA forward 5'-GGATAAGATGGAAACTTCTGACA-3'

RIG-I sgRNA reverse 5'-GGCCTGAAGATCCTCCAAGT-3'

MDA5 sgRNA forward 5'-TGGTTGGACTCGGGAATTCG-3'

MDA5 sgRNA reverse 5'-CGAATTCCCGAGTCCAACCA-3'

IPS-1 sgRNA forward 5'-CCTGGTGCAGTGCCTTCTA-3'

IPS-1 sgRNA reverse 5'-GTGACTACCAGCACCCCTGT-3'

IRF-3 sgRNA forward 5'-TCCACCATTGGTGTCCGGAG-3'

IRF-3 sgRNA reverse 5'-CTCCGGACACCAATGGTGGA-3'

IFNAR1 sgRNA forward 5'-CACCAAGCAGCACTACTTACGTCA-3'

IFNAR1 sgRNA reverse 5'-TGACGTAAGTAGTGCTGCTTCAAA-3'

PKR sgRNA forward 5'-CAGTGTGCATCGGGGGGTGCAGTTT-3'

PKR sgRNA reverse 5'-TGCACCCCCGATGCACACTGCGGTG-3'

TRIF sgRNA forward 5'-ATGAGGCCCGAAACCGGTGTGGG-3'

TRIF sgRNA reverse 5'-CCCACACCGGTTTCGGGCCTCAT-3'

GFP-IRF-3 and GFP-Δ1-58IRF-3 constructs were created by inserting coding sequence of IRF-3 (1-427) or (59-427), respectively, into the pAcGFP1-C1 expression vector (Clontech). HeLa cells stably expressing GFP-IRF-3 and GFP-Δ1-58IRF-3 were generated by

transfecting respective expression vectors into IRF-3 KO HeLa. 48 h after transfection, cells were first collected and sorted by GFP using SH800S Cell Sorter (SONY). GFP positive cells were harvested and grown in 10-cm dish for 24 h, and then selected again by G418 (Nacalai Tesque) for Neomycin resistance in 10-cm dishes for two weeks, followed by single-cell clone selection in 98-well plate. pC939 GyrB-PKR and pC940 GyrB-PKR K296H plasmid were kindly provided by Dr. Tom Dever (Ung et al., 2001) . These plasmids were co-transfection with selection marker (pIRES puro2, Clontech) into PKR KO HeLa cells. 48 h after transfection, cells were selected by puromycin (InvivoGen) for two weeks, followed by single-cell clone selection in 98-well plate. HeLa cells stably expressing GyrB-PKR and FK-IPS-1 were generated by transfecting FK-IPS-1 plasmid (with Neomycin resistance gene) into GyrB-PKR HeLa cells, cells were then treated with G418 for two weeks followed by single-cell clone selection in 98-well plate. FK-IPS-1 construct were previously described (Takamatsu et al., 2013). The cFLIP expression vector was created by inserting the coding sequence of full-length cFLIP into the pEF-BOS(+) vector (Mizushima & Nagata, 1990) by the following primers,

cFLIP forward: 5'-ATGTCTGCTGAAGTCATCCA-3'

cFLIP reverse: 5'-TTATGTGTAGGAGAGGATAAG-3'

2.2   Microinjection and live cell imaging

Step 1 Seeding:

1. 48 h prior to injection, cells were seeded at 1×10^5 on a grid-imprinted cover glass (Matsunami Glass #GC1310) placed in a 35-mm culture dishes (Greiner Bio-One) with c-DMEM.

Step 2 Photographing:

2. 2 h prior to injection, cell-seeding cover glass was transferred carefully by forceps into a μ-Dish[35mm high] plate (ibidi) containing 1 ml of 37°C pre-warmed PBS. Single cell derived colonies, each with 8-32 non-dividing cells, were selected and their locations were recorded under a confocal microscope (Leica TCS SP8). Images taken at this time point were annotated as (0 h). After photographing, cover glass was immediately transferred back to the c-DMEM and the incubator.

Step 3 Preparing for injection:

3.1 During injection, cell-seeding cover glass were transferred carefully by forceps into an injection plate with 400 µl c-DMEM. Microinjection were conducted manually using Leica MICROSYSTEMS with self-made glass needle (radius <0.5 µm) at room temperature (RT). All injection substrates were centrifuged at 12,000×g, 4℃, 10 min, and 2 µl of the substrate were loaded into the injection glass needle by micro-tips (Eppendorf), glass needle was then tapped gently to avoid air bubbles.

3.2 Next, the glass needle was connected to the injection pump (FemtoJet, Eppendorf), before formal injection, the glass needle was tested for its permeability by flushing in c-DMEM for a few seconds. The needle was ready to use when the clear stream of substrates could be observed during the flashing.

3.3 Using neighboring cells, the ideal injection pressure for the substrate was optimized. Subsequent injections were performed under a pressure that permits a modest stream of the substrate to enter the cell cytoplasm without damaging the cell body.

3.4 Selected colonies were retrieved and injected by one shot. After the injection, the cover glass was transferred back to the culture dish with c-DMEM in the incubator.

Step 4 Observing:

4. At desired time points after injection, cell seeding cover glass were photographed as described in step 2 to observe the localization of IRF-3 and the apoptosis condition in live cells.

Notes

The workflow of microinjection is briefly depicted in illustration. 3.

At least three independent repeats of each injection experiment were completed. 3-6 colonies were injected for each substrate and in each repeat. Concentrated poly I:C and proteins needed greater injection pressures of roughly 150-180 hundred pascals (hPa), while PBS can be easily injected at a pressure around 80 hPa. Cell bursting was triggered by an excessive injection pressure, as shown in Figure 2B. The average injection volume by one shot was estimated as one-tenth of the total cell volume. The radius of an attached HeLa cell is roughly 12.5 µm, taking into account the hemispherical shape of the cell, the average

volume of the injected substrate was estimated to be $(\pi \times 12.5^2) \times 1/2 \times 1/10) \approx$ 24.5 fl.

2.3 Preparation of injection substrates

(GG25) is a short dsRNA with 5 end triphosphate overhang, the structure of GG25 was described in (Takahasi et al., 2008) . GG25 was produced using the AmpliScribe™ T7-Flash™ Transcription Kit (Epicentre) according to the manufacturer's protocol with the dsDNA template created by annealing of two synthetic DNA oligos:

5'-TAATACGACTCACTATA-3' and

5'-CACTTTCACTTCTCCCTTTCAGTTTCCTATAGTGAGTCGTATTA-3'.

10μl 10x M buffer, 40μl DNA oligo each (100uM) and 10μl nuclease free water were mixed and incubated at 95℃ for 5 min, then cooled down at RT for 30 min.

The following ingredients were mixed at RT in the below order and incubated for 4 h: 5μl of T7 enzyme solution, 5μl of 10x reaction buffer, 5μl of DTT, 4.5μl of ATP, GTP, CTP, and UTP each, 10μl of annealed GG25 DNA template, 5.75μl of nuclease free water, and 1.25μl of RNase inhibitor. DNase I was used to digest the reaction after incubation, and RNA was then purified using phenol/chloroform extraction, followed by Mini Quick Spin Columns (Roche) to remove NTP residues, and finally with ethanol precipitation (See detail in the section of RNA purification). GG25 was aliquoted and stored at -80℃.

(Poly I:C) was purchased from GE Healthcare, the length of poly I:C ranges from several hundreds to kilos base pairs. Poly I:C was aliquoted and stored at 4℃.

(Recombinant RIG-I) was produced in High Five cells by infecting recombinant baculovirus and purified as described in previous study (Saito et al., 2007). Recombinant RIG-I protein was aliquoted and stored at -80℃.

(Recombinant ΔTM-IPS-1) was produced from Escherichia coli expressing ΔTM-IPS-1 and purified as described in previous study (Takahasi et al., 2019). Recombinant ΔTM-IPS-1 protein was aliquoted and stored at -80℃.

(Recombinant MDA5 wt/GS) was produced in High Five cells by infecting recombinant baculovirus and purified as described in previous study (Duic et al., 2020)

(RIG-I+GG25) mixture was made by mixing (1 μg/μl each) followed by a 30 min

incubation at 37°C prior to the injection.

(Rb-dsRNA) the genome of *Endornavirus* in rice was extracted from rice bran as described in previous study (Kasumba et al., 2017). Rb-dsRNA was aliquoted and stored at -80°C.

2.4   Chemical reagents

Dimethyl sulfoxide (DMSO), Cycloheximide (CHX), and chloroquine were purchased from Nacalai Tesque, Coumermycin A1 was purchased from Promega, human TNF-α was purchased from PeproTech, AP20187 was purchased from ARIAD Pharm, Z-VAD was purchased from R&D Systems, NH_4Cl was purchased from SI Science, and human IFN-β was purchased from Sigma.

2.5   Immunoblotting

Cells were harvested in cold PBS and lysed on ice with RIPA buffer containing a protein inhibitor cocktail (1:1000) (150 mM NaCl, 50 mM Tris-HCl pH 7.5, 1 % NP40, 0.5 % DOC, and 0.5 % SDS). Cell lysate was incubated at 4°C for 30 minutes and centrifuged (16,000×*g*, 4°C, 10 min) to removed cell pellet. The supernatant was gathered and subjected to SDS-PAGE or native-PAGE (IRF-3 dimerization). Proteins were transferred to an Immobilon-P PVDF membrane (Millipore) by a transfer machine. The membrane was then blocked in TBS-T with 5% skim milk (blocking buffer) at RT for 30 min. Primary antibodies were diluted 1:1000 or 1:500 (cFLIP) in blocking buffer and incubated with the membrane in plastic bags at 4°C for overnight or RT for 2 h (cFLIP). Horseradish peroxidase (HRP)-conjugated secondary antibodies were diluted 1:3000 in blocking buffer and incubated at RT for 1 h. Protein bands were detected using Chemi-Lumi One Super (Nacalai Tesque) and photographed by LAS-4000 instrument (Fujifilm).

anti-IRF-3 mouse mAb (CBX-CBX00167) was purchased from Cosmo Bio; anti-cFLIP mouse mAb (#ALX-8040961-0100) was purchased from Enzo Life Sciences; anti-PKR mouse mAb (#sc-6282), anti-GAPDH mouse mAb (#sc-32233) were purchased from Santa Cruz Biotechnology; anti-TRIF rabbit mAb (#4596S) anti-PARP rabbit mAb (#9542S), anti-caspase 8 mouse mAb (#9745S), anti-caspase 9 rabbit mAb (#9502S), HRP-linked anti-mouse IgG (#7076S), and HRP-linked anti-rabbit IgG (#7074S) were purchased from Cell Signaling Technology,

2.6 Transfection and siRNA

24 h prior to transfection cells were seeded in 6-well or 12-well plate at 50% confluency. Cells were first washed with PBS. GG25, poly I:C and expression vectors were transfected with Lipofectamine 2000 (Invitrogen) in Opti-MEM (Gibco). siRNA was transfected with Lipofectamine RNAiMAX (Invitrogen) in Opti-MEM. siRNA for cFLIP, PKR and control RNA were purchased from Applied Biosystems. Before transfection, cells were carefully washed by PBS to remove P/S.

2.7 Viral infection and titration

24 h prior to infection cells were seeded on 12-well plate (2×10^5 cells/well).

Following a PBS wash, the cells were infected with either SeV (3.2×10^2 HAu/ml) or SINV (MOI=1). After an hour of infection, the virus-containing medium was removed and 500 µl of fresh c-DMEM was added. At the appropriate time points, supernatants were collected for viral titration.

Hemagglutination assay (HA) was performed using chicken erythrocytes (Japan Bio Science Laboratory) for titration of SeV. The virus-containing supernatant was 2-fold serially diluted (50 µl/well) in a 96-well round-bottomed microplate. The supernatant was then mixed with 0.5% fresh erythrocyte suspension (50 µl/well). The reaction (100 µl/well) was incubated at RT for 1 h, and the first dilution factor under which erythrocyte formed aggregates was recorded.

Plaque assay was performed using Vero cells for the titration of SINV. 24 h prior to titration, Vero cells were seeded in 24-well plates at 1×10^5/well. Vero cells were infected with (10-fold serially diluted) virus-containing supernatant in c-DMEM. One hour after infection, virus-containing medium was removed, and 1 ml/well of fresh c-DMEM containing 1.5% Avicel (Sigma) was gently added. 48 h after infection, c-DMEM containing Avicel was carefully removed, cells were washed by PBS, and then fixed with 4% PFA at RT for 15 min. Finally, the plate was stained by crystal violet (Nacalai Tesque) on a shaker at RT for 20 min. Plates were then washed, dried, and subjected to plaque counting.

2.8 RNA fluorescence in situ hybridization (FISH)

At a chosen time after microinjection, the cell-seeding cover glass were carefully transferred to a 24-well plate containing 500 µl PBS by forceps, and then fixed with 4% PFA (300 µl/well) at RT for 15 min. Cover glass was washed twice with 500 µl of PBS after the PFA fixation, 300 µl of 0.1% Triton X-100 in PBS were added to permeabilize the cell membrane for 15 min, cell were then washed by PBS again prior to FISH staining. FISH was conducted by using a kit (Affymetrix) in accordance with the manufacturer's protocol. In brief, cells were incubated with the following ingredients orderly. **1.** human *IFNB* probe (1:100) in probe set buffer (3 h). **2.** Pre-amplifier buffer (1 h). **3.** Amplifier buffer (1 h). **4.** label probe (1:25) in label buffer (1 h). All incubation steps were performed at 40°C in a light proof shaker. Between each step, cells were washed by FISH washing buffer for three times (5 min/each). Finally, cells were stained with DAPI (1:1000) in PBS at RT for 10 min and cleaned with PBS. Cover glass was mounted on a glass slide and imaged with Leica TCS SP8 confocal microscope.

2.9 Immunostaining

Cells subjected to immunostaining were fixed and permeabilized as described in the FISH section. Cells were blocked with PBS-T containing 1% BSA and 5% glycerol (blocking buffer) at 4°C for 30 min. Primary antibodies were added (1:500) to blocking buffer and incubated with cells at RT for 1 h or 4°C for overnight, followed by three washes with PBS-T (10 min each). Secondary antibodies were added (1:1000) to blocking buffer and incubated at 4°C for 1 h, followed by three washes with PBS-T (10 min each). Nucleus were stained with DAPI (1:1000) in PBS-T at RT for 10 min and rinsed by PBS-T. Cells were imaged with Leica TCS SP8 confocal microscope.

Antibodies used for immunostaining were listed below:

Anti-IRF-3 rabbit pAb were produced as described in previous study (Yoneyama et al., 1998) ; anti-G3BP1 mouse mAb (#sc-365338), anti-TIAR goat pAb (#sc-1749) were purchased from Santa Cruz Biotechnology; Alexa Fluor 488 donkey anti-rabbit, Alexa Fluor 594 donkey anti-mouse, and Alexa Fluor 647 donkey anti-goat were purchased from Life Technologies.

2.10 Cell survival quantification

1. Survival of injected cells was calculated using the following formula:

$$\text{Cell survival} = \left(1 - \frac{b}{a}\right) \times 100\%$$

a= the total number of injected cells (deduct mechanical cell death)

b= the number of currently surviving cells

2. Cells subjected to survival quantification by Amido black staining were gently washed with PBS and fixed with 4% PFA at RT for 15 min. Amido black solution was stained at RT for 30 min on a shaker, and then dried for overnight. For quantification, cells were first washed by 0.3 M CH₃COONa (pH 5.6) to clean the excessive staining. Amido black was extracted from each sample by 300 µl of 50 mM NaOH. Amido black absorbance was measured at 630 and 405 nm by a microplate reader (Bio-Rad). OD630 - OD405 was calculated as the Amido black intensity (ABI) and used to present cell survival.

2.11 RNA extraction and real time-qPCR

Before RNA extraction, cells were washed by 1xPBS and collected with 500µl TRIzol reagent at RT. 100µl chloroform (1:5 to the TRIzol volume) were mixed with the homogenized cell sample and centrifuged at 12,000×g, 4℃, 10 min. Upper phase of the sample was collected and added with 250µl isopropanol (1:2 to TRIzol volume). Samples were then incubated at RT for 10 minutes and centrifuge at 12,000×g, 4℃, 10 min. The supernatant was then removed and gently washed by 500µl 70% ethanol, followed by centrifuge at 12,000×g, 4℃, 5 min. The supernatant was removed again, and the RNA pallet was air dried at RT for 5 min. RNA pallet was then dissolved in 200µl nuclease free water and added with same volume of PCI solution (phenol:chloroform:isoamyl alchohol=25:24:1), and centrifuged at 12,000×g, 4℃, 10 min. The upper phase of the sample was collected in a new tube and added with the same volume of CIA solution (chloroform:isoamyl alchohol=24:1), and centrifuged again at 12,000×g, 4℃, 10 min. The upper phase of the sample was collected and added with 400 µl 100% ethanol, 20µl 3M sodium acetate, and incubated at -80℃ for more than 30 min. -80℃ incubated sample was

thawed and centrifuged at 12,000×*g*, 4℃, 10 min. The supernatant was removed, and RNA pellet was washed by 70% ethanol followed by centrifuge at 12,000×*g*, 4℃, 5 min. Finally, the supernatant was removed, and the RNA pellet was air dried at RT for 10 min. The pellet was then dissolved in 50μl nuclease free water in 55℃ for 10 min and quantified by NanoDrop (Eppendorf). RT-qPCR was conducted using 65℃ denatured RNA yielded from the above procedure. High-capacity cDNA reverse transcription kit (Applied Biosystems) was used for reverse transcription. cDNA was amplified with the Fast SYBR green master mix (Applied Biosystems) on a Step One Plus real-time PCR system (Applied Biosystems) SYBR green primers used in the present study were:

h-GAPDH forward: 5'-CTGCACCACCAACTGCTTAG-3'

h-GAPDH reverse: 5'-GTCTTCTGGGTGGCAGTGAT-3'

h-IFNB forward: 5'-AGTCTCATTCCAGCCAGTGC-3'

h-IFNB reverse: 5'-AGCTGCAGCAGTTCCAGAAG-3'

h-cFLIP forward 5'-CTGGTTGCCCCAGATCAACT-3'

h-cFLIP reverse 5'-CCCAGGGAAGTGAAGGTGTC-3'

2.12   Statistical analysis

Statistical analyses were performed with the help of GraphPad Prism, data represent means ± SEM, and the significance is shown as *$P < 0.05$, **$P < 0.01$, ***$P < 0.001$, ****$P < 0.0001$, and ns: not significant. Images of microscopy and immunofluorescence are typical results of at least three independent experiments.

CHAPTER 3

RESULTS

3.1 Cytoplasmic injection of RNA/protein triggers IRF-3 nuclear translocation and subsequent *IFNB* gene production.

In vitro transcribed 5'-ppp-RNA (GG25) and dsRNA mimic poly I:C were shown to induce robust IRF-3 activation and *IFNB* gene expression upon transfection (Takahasi et al., 2008). To test whether microinjection of RNA and proteins resulted in similar outcome, we generated HeLa cells lacking endogenous IRF-3 and expressing GFP-conjugated IRF-3 to visualize IRF-3 localization in real time. GFP-IRF-3 HeLa cells were injected with RNAs or proteins of interests, and each cell was followed by live imaging of GFP signal. The image of IRF-3 nuclear translocation triggered by injection of poly I:C at 3h is described in (Figure. 1A). A percentage of nuclear IRF-3 induced by injection of various stimuli were summarized in (Figure. 1B). Injection of PBS, a negative control, did not change IRF-3 cytoplasmic localization. Poly I:C injection induced remarkable nuclear IRF-3 from 89% to 96% with the induction of its concentration. However, injection of GG25 only induced nuclear IRF-3 in a small portion of cells up to 25%. To enhance GG25 triggered signaling by injection, treatment of IFN-β was applied prior to GG25 injection. RIG-I was known as a potent ISG upregulated during IFN-β production, and as a result, pre-treatment of IFN-β markedly increased nuclear IRF-3 upon GG25 injection (96%). Similarly, injection of recombinant RIG-I protein, which resulted in no IRF-3 activation, significantly enhanced IRF-3 activation when co-injected with GG25 (93%). These results supported that induction of RIG-I level promoted the sensing of GG25. Additionally, ΔTM-IPS-1 protein effectively induced IRF-3 activation by injection, which agrees with the previous finding showing that ΔTM-IPS-1 can activate IRF-3 dimerization during *in vitro* incubation with cell extract, which induces endogenous IPS-1 aggregation for downstream signaling (Hou et al., 2011). A clear IRF-3 translocation was induced by microinjected RNA and proteins, and further *IFNB* gene expression was also confirmed in IRF-3 translocated cells by fluorescence *in situ* hybridization (FISH) assay (Figure. 1C). Moreover, injection of GG25 alone exhibited significant less *IFNB* signal comparing to RIG-I+GG25 co-injection (Figure. 1D, E). Collectively these results confirmed that cytoplasmic delivering of RNA/protein by microinjection triggered rapid and authentic cellular responses, and thereby, it served as a powerful system for single-cell analysis.
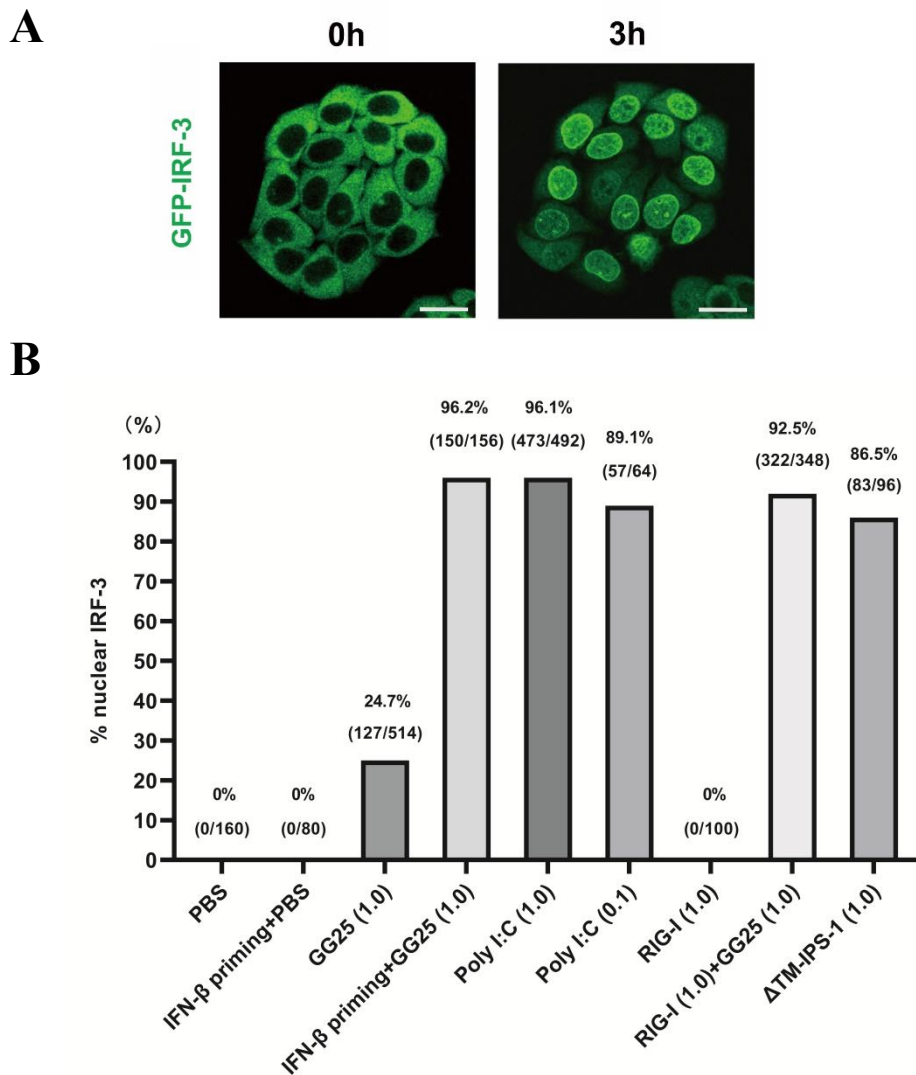
Figure 1. The cytoplasmic RNA/protein injection induces prompt and potent cellular responses.
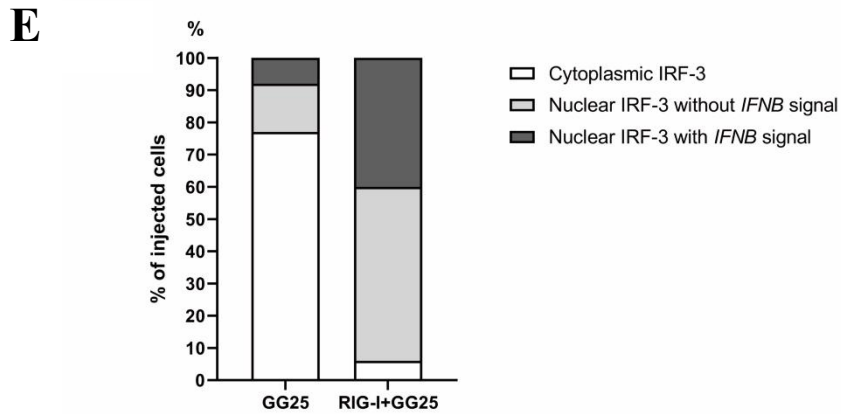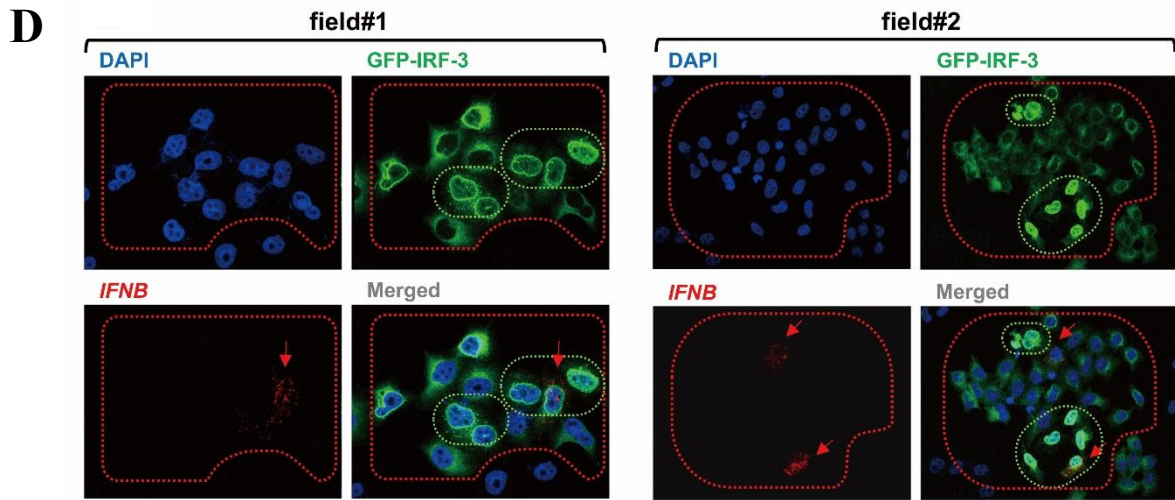**A**: GFP-IRF-3 HeLa cells were injected with poly I:C (1 μg/μl) and observed by live cell imaging for the localization of IRF-3 at the indicated times after the injection. The injection was performed in a colony of cells, and each infected cell was followed for the nuclear translocation of IRF-3. The % of nuclear translocated IRF-3 was calculated (number of cells with nuclear IRF-3/number of injected cells). Scale bar = 25 μm
B: GFP-IRF-3 HeLa cells were injected with the indicated RNA/protein. GG25: 5'-ppp-RNA; poly I:C: long poly I:C; RIG-I: recombinant RIG-I protein; ΔTM-IPS-1: recombinant IPS-1 protein deleted of the transmembrane domain. The amount of injected RNA or protein (μg/ml) is indicated at the bottom of the chart. IFN-β priming represents the pretreatment of IFN-β (1000 U/ml for 12 h) to cells prior to the injection. Injected cells were observed live at 3 h after injection for the localization of IRF-3, and the % nuclear IRF-3 was calculated as in (A) and shown at the top of each bar.
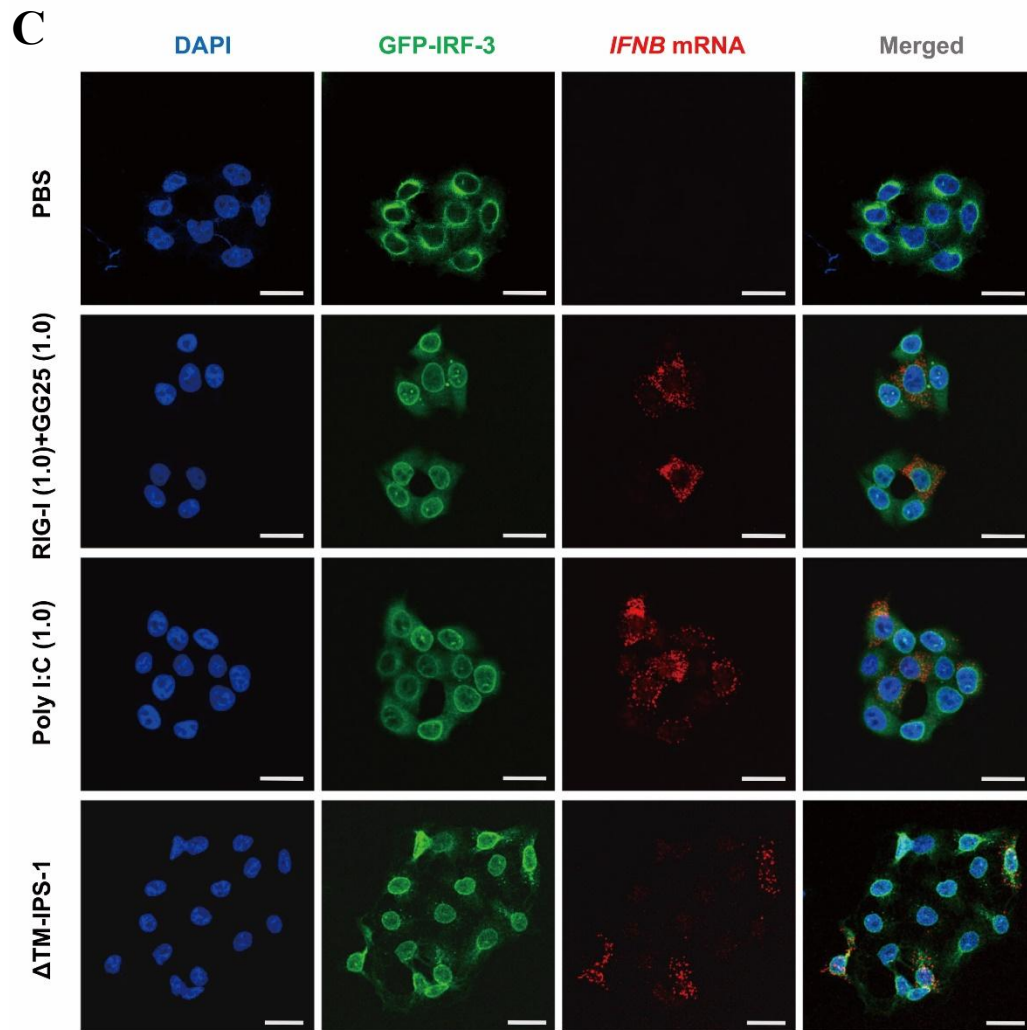
Figure 1. The cytoplasmic RNA/protein injection induces prompt and potent cellular responses.
C: GFP-IRF3 HeLa cells were injected with the indicated RNA/protein. 3 h after injection cells were fixed and observed for IRF-3 (green) or the expression of *IFNB* mRNA by FISH (red). Scale bar = 25 μm

D

field#1

| DAPI | GFP-IRF-3 |
| IFNB | Merged |

field#2

| DAPI | GFP-IRF-3 |
| IFNB | Merged |

E

□ Cytoplasmic IRF-3
□ Nuclear IRF-3 without *IFNB* signal
■ Nuclear IRF-3 with *IFNB* signal

Figure 1. The cytoplasmic RNA/protein injection induces prompt and potent cellular responses.

D: GFP-IRF-3 HeLa cells were injected with GG25 (1 µg/µl) alone. Cells were fixed after 3 h and observed for IRF-3 (green) or the expression of *IFNB* mRNA (FISH, red). Cells encircled in red are injected cells. Cells encircled in green show nuclear IRF-3. Arrows indicate cells positive for *IFNB* mRNA. Scale bar = 25 µm

E: GFP-IRF-3 HeLa cells injected with GG25 alone or RIG-I+GG25 were analyzed as in b and quantified for the localization of IRF-3 and expression of *IFNB* mRNA.

3.2 Apoptotic cell death induced by the cytoplasmic injection of RNA/protein.

Microinjection has been confirmed to induce rapid cellular response including IRF-3 and *IFNB* activation. And further analysis of cell fate induced by different RNA by injection was of interest. GFP-IRF-3 HeLa cells injected with poly I:C exhibited efficient IRF-3 nuclear translocation and these cells went through robust cell death within 6 h (Figure. 2A), yet PBS did not induce cell death by injection. Injection with high influx pressure sometimes caused mechanical damage and resulted in rapid burst-like cell death (Figure. 2B). However, mechanical damage caused cell death is shown with the loss of cytoplasmic contents, including GFP-IRF-3, and is morphologically distinct from that induced by RNAs (Figure 2C). Cells were next injected with RIG-I + GG25 to examine the cell death pattern triggered by RIG-I signaling (Figure. 2D). These cells also exhibit IRF-3 nuclear translocation and cell death; however, in contrast to that induced by poly I:C injection, it is with slow kinetics and lower efficiency (Figure. 2D). Moreover, in surviving cells, nuclear IRF-3 showed its re-location back to cytoplasmic area at 16-24 h (Figure. 2D). Cells were then treated with Z-VAD, a pan-caspase inhibitor to analyze the type of cell death induced by RNA (Figure. 2E). In Z-VAD pre-treated cells poly I:C induced efficient IRF-3 nuclear translocation but with no cell death over 12 h of injection. This result confirmed that the cell death induced by cytoplasmic poly I:C injection was apoptosis. To examine whether the cytoplasmic delivering of RNA by the method of transfection resulted in a similar outcome, GFP-IRF-3 HeLa cells were transfected with these RNA using lipofectamine (Figure. 2F). Transfection of poly I:C induced marked apoptosis within 24 h, whereas that of GG25 only induced limited cell death. IFN-β priming, which is known to elevate RIG-I expression, promoted cell death upon GG25 transfection (Figure. 2G). Similarly, IFN-β priming also enhanced poly I:C transfection-induced cell death to some degree (Figure. 2H). However, the cell death kinetics induced by GG25 and poly I:C were consistent to be slow and fast, respectively, irrespective of IFN-β priming. These results suggested that poly I:C and GG25 induce cell death via distinct mechanisms. In contrast to injections, treatment of exogenous poly I:C induced nuclear translocation of IRF-3, but not significant cell death in HeLa cells (see below). Therefore, in response to different types of cytosolic RNA, distinct cell fate was induced by a series of physiological signals.
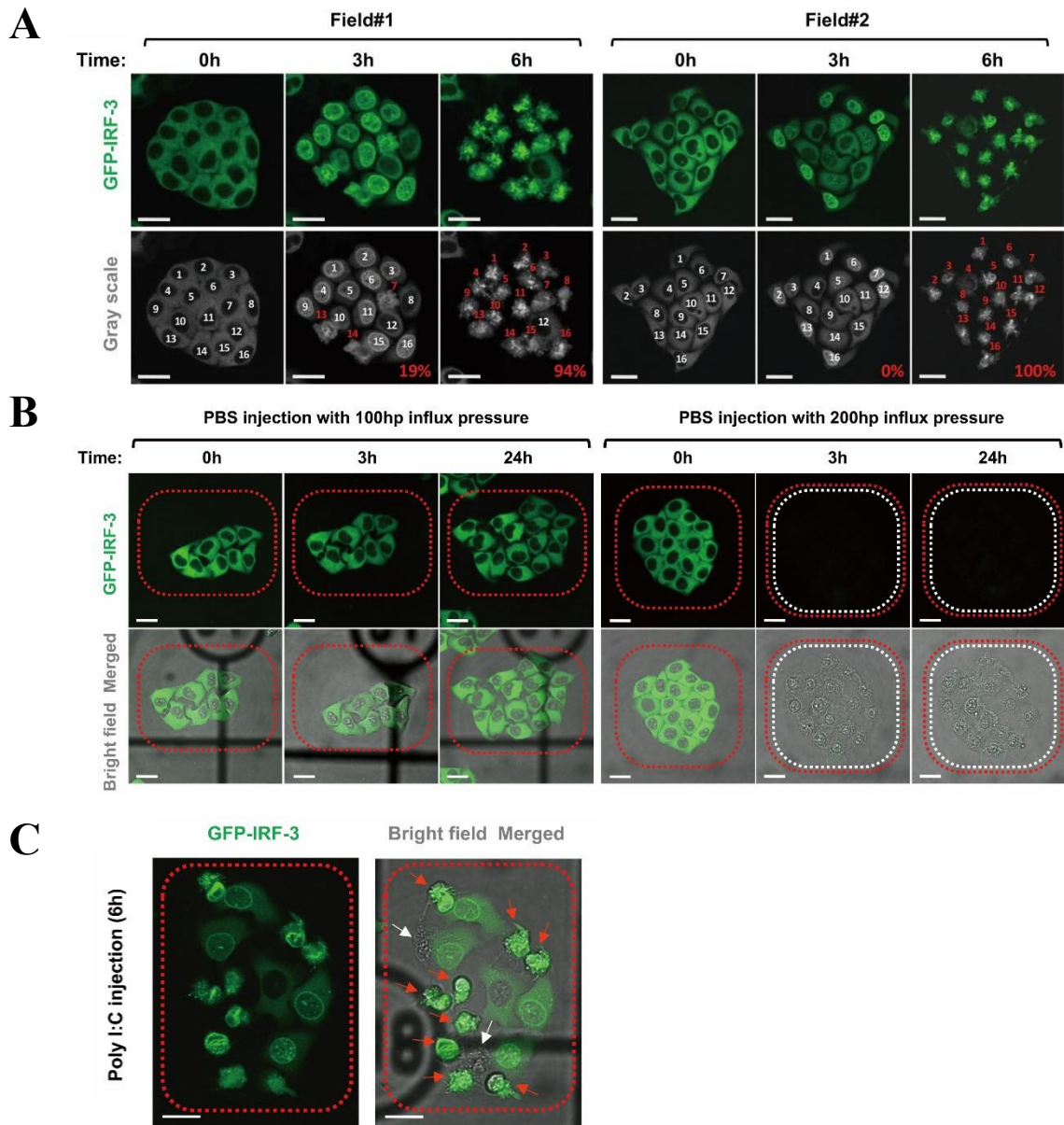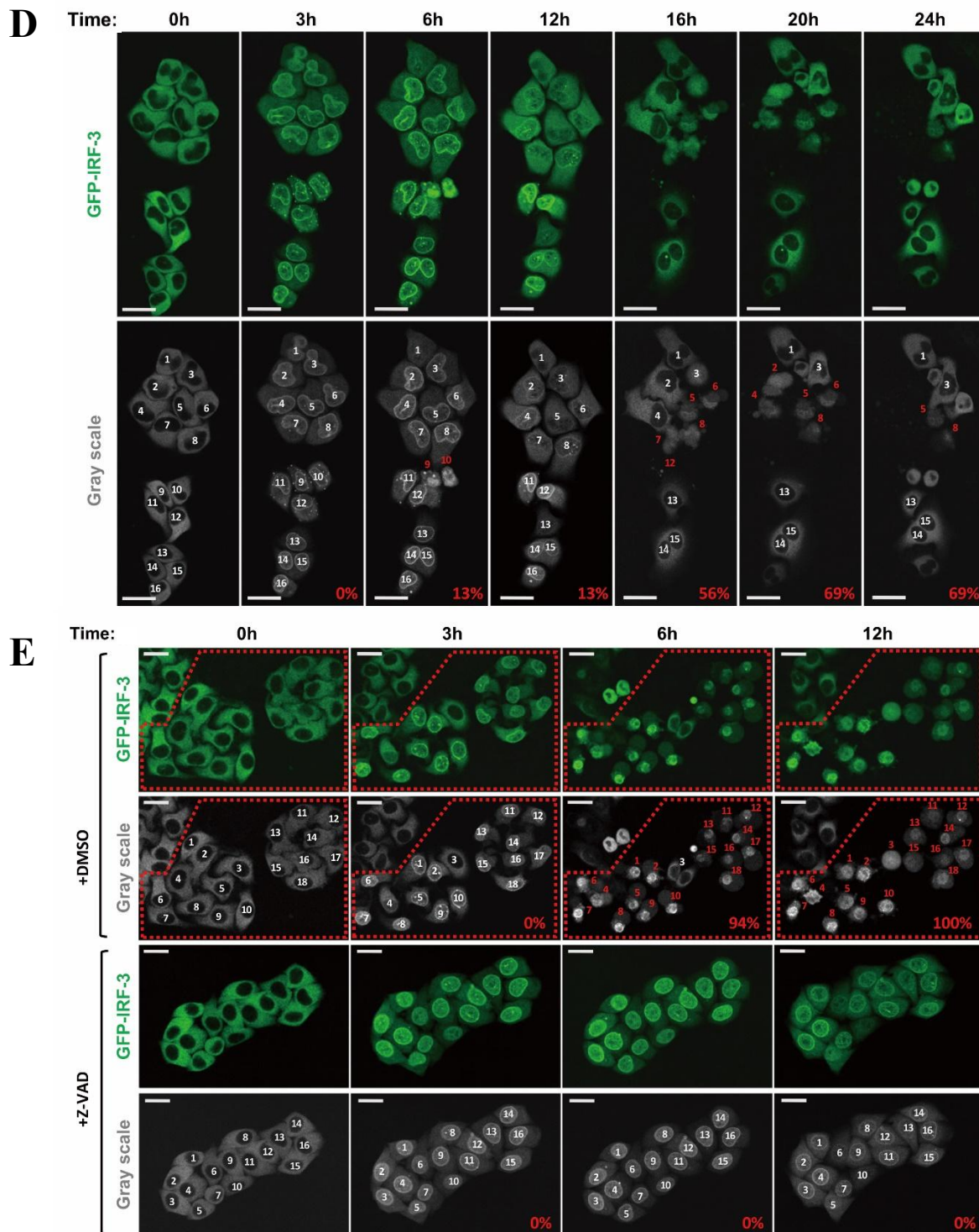
Figure 2. Induction of the nuclear translocation of IRF-3 and subsequent apoptosis by the cytoplasmic injection of RNA/protein.

A: GFP-IRF-3 HeLa cells were injected with poly I:C (1 µg/µl) and observed live for the localization of IRF-3 at the indicated times after the injection. Injected cells were numbered (white) and followed; cells with red numbers exhibited morphological cell death; % of dead cells was calculated (as depicted in gray scale images).

B: GFP-IRF-3 HeLa cells were injected with PBS at a low (100 hPa) or high (200 hPa) influx pressure and observed live for GFP and cell death. Injected cells are encircled in red. Cells that died due to a high influx pressure are encircled in white.

C: GFP-IRF-3 HeLa cells were injected with poly I:C (1 µg/µl) and observed live for different types of cell death. Injected cells are encircled in the red. RNA-induced dead cells are shown by red arrows. Cells that died due to mechanical stress are indicated by white arrows. Scale bar = 25 µm

Figure 2. Induction of the nuclear translocation of IRF-3 and subsequent apoptosis by the cytoplasmic injection of RNA/protein.

D: GFP-IRF-3 HeLa cells were injected with RIG-I and GG25 (1 µg/µl each) and observed as in (A)

E: GFP-IRF-3 HeLa cells were injected with poly I:C (1 µg/µl) in the absence (DMSO) or presence of Z-VAD (20 µM) and observed as in (A). Z-VAD was added 3 h prior to the injection and kept in the culture medium. Injected cells are indicated in the red dotted box. Scale bar = 25 µm
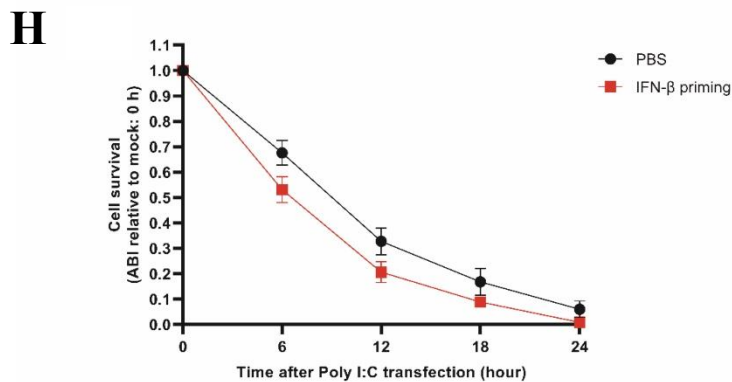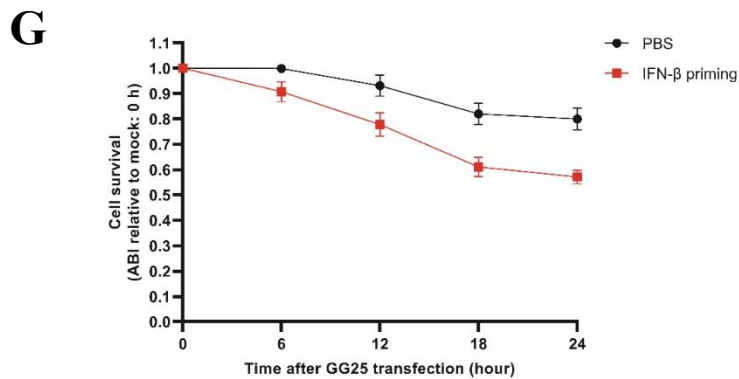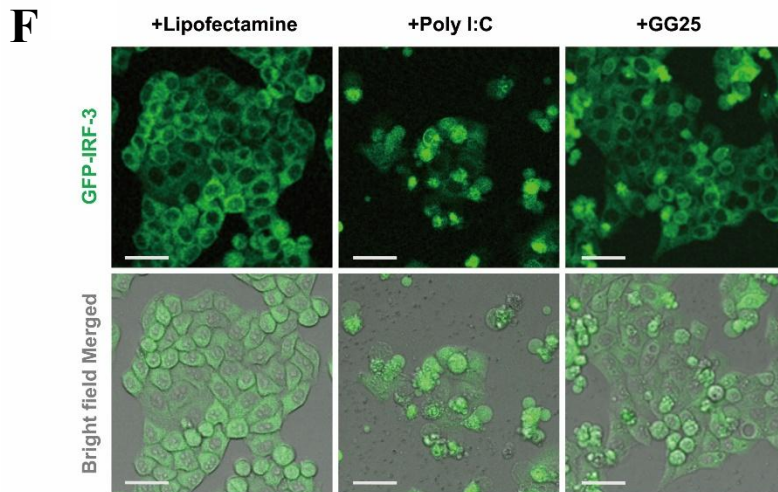
Figure 2. Induction of the nuclear translocation of IRF-3 and subsequent apoptosis by the cytoplasmic injection of RNA/protein.

F: GFP-IRF-3 HeLa cells were mock transfected (lipofectamine only) or transfected with poly I:C (0.5 μg/ml, 24 h) or GG25 (4 μg/ml, 24 h) with lipofectamine and observed for cell death. Scale bar = 50 μm

G: HeLa cells were pre-treated with culture medium with or without IFN-β (1000 U/ml) for 12 h, transfected with GG25 (4 μg/ml), and examined for cell survival at the indicated time points.

H: HeLa cells were pre-treated with culture medium with or without IFN-β (1000 U/ml) for 12 h, transfected with poly I:C (0.5 μg/ml), and examined for cell survival at the indicated time points. Data in (G) (H) are represented as the means ± SEM of two independent experiments.

3.3 Diverse cell death mechanisms induced by GG25 and poly I:C.

To characterize the mechanistic differences underlying cell death induced by RIG+GG25 and poly I:C, different RNA signaling components were examined for their role in cell death induction. IRF-3 nuclear translocation was often observed prior to apoptosis upon RNA injection, however, its role in this process is not clearly understood. Δ1-58IRF-3 (DNA binding domain deleted) exhibits no transcriptional activity and functions as a dominant inhibitor (Yoneyama et al., 1998). GFP-Δ1-58IRF-3 was expressed in IRF-3 KO HeLa cells (GFP-Δ1-58IRF-3 HeLa) (Figure. 3A, B; Figure. S3A) to test the effect of IRF-3 function in apoptosis induction. GFP-IRF-3 HeLa and GFP-Δ1-58IRF-3 HeLa cells were injected with RIG-I+GG25 and examined for cell death (Figure. 3C). Limited cell death was observed in GFP-IRF-3 HeLa cells as described in Figure. 2D, however, cell death was absent in GFP-Δ1-58IRF-3 HeLa cells. Furthermore, cell death was also inhibited by deleting IFNAR1 (GFP-IRF-3 IFNAR1 KO HeLa). Similarly, GG25 transfection induced marked cleavage of PARP in GFP-IRF-3 HeLa cells; however, that was significantly attenuated in GFP-Δ1-58IRF-3 and GFP-IRF-3 IFNAR1 KO HeLa cells (Figure. 3D). These results suggested that cell death signal driven by RIG-I was largely dependent on IRF-3 transcriptional activity and the secreted IFN-I, which is consistent with the slow kinetics of cell death observed after RIG-I+GG25 injection. In contrast, when poly I:C was injected to GFP-Δ1-58IRF-3 and GFP-IRF-3 IFNAR1 KO HeLa cells robust cell death was induced, suggesting that cell death triggered by poly I:C was independent of IRF-3 activation and further IFN-I production (Figure. 3E). To systemically investigate the participation of signaling components in cell death, HeLa cells with knock out of RIG-I, MDA5, IPS-1, IRF-3, IFNAR1, or PKR were generated. Cell death pattern induced by poly I:C injection was not changed except for PKR KO HeLa (Figure. 3F), suggesting that poly I:C induced cell death went through a PKR dependent, but RLR or IFN-I signaling independent pathway. Similar results were shown by the transfection of poly I:C (Figure. 3G). Furthermore, by injecting rice Endornavirus dsRNA (rb-dsRNA) isolated from rice bran (Kasumba et al., 2017), the cell death induced by poly I:C was proved not to be caused by the synthetic nature of poly I:C itself (Figure. 3H). Next, the activation of PKR was confirmed by detecting SG formation under the stimulation of different RNA via

different methods (Figure. 3I). In HeLa cells, exogenous treatment of poly I:C without a transfection reagent induced efficient IRF-3 nuclear translocation, however, SG containing TIAR and G3BP1 were not induced as cytoplasmic granules. In contrast, intracellular delivering of poly I:C by either injection or transfection induced the nuclear translocation of IRF-3 and SG formation. These findings further supported PKR being critical in poly I:C injection or transfection induced cell death, and are consistent with that treatment of poly I:C induced neither SG nor cell death. Additionally, IRF-3, but not SG were induced by injection or transfection of GG25, indicating that cell death induced by poly I:C and GG25 underwent distinct mechanisms. As a rapid and robust cell death was induced by dsRNA mimic poly I:C, we thereafter focused on the mechanisms underlying this phenomenon.
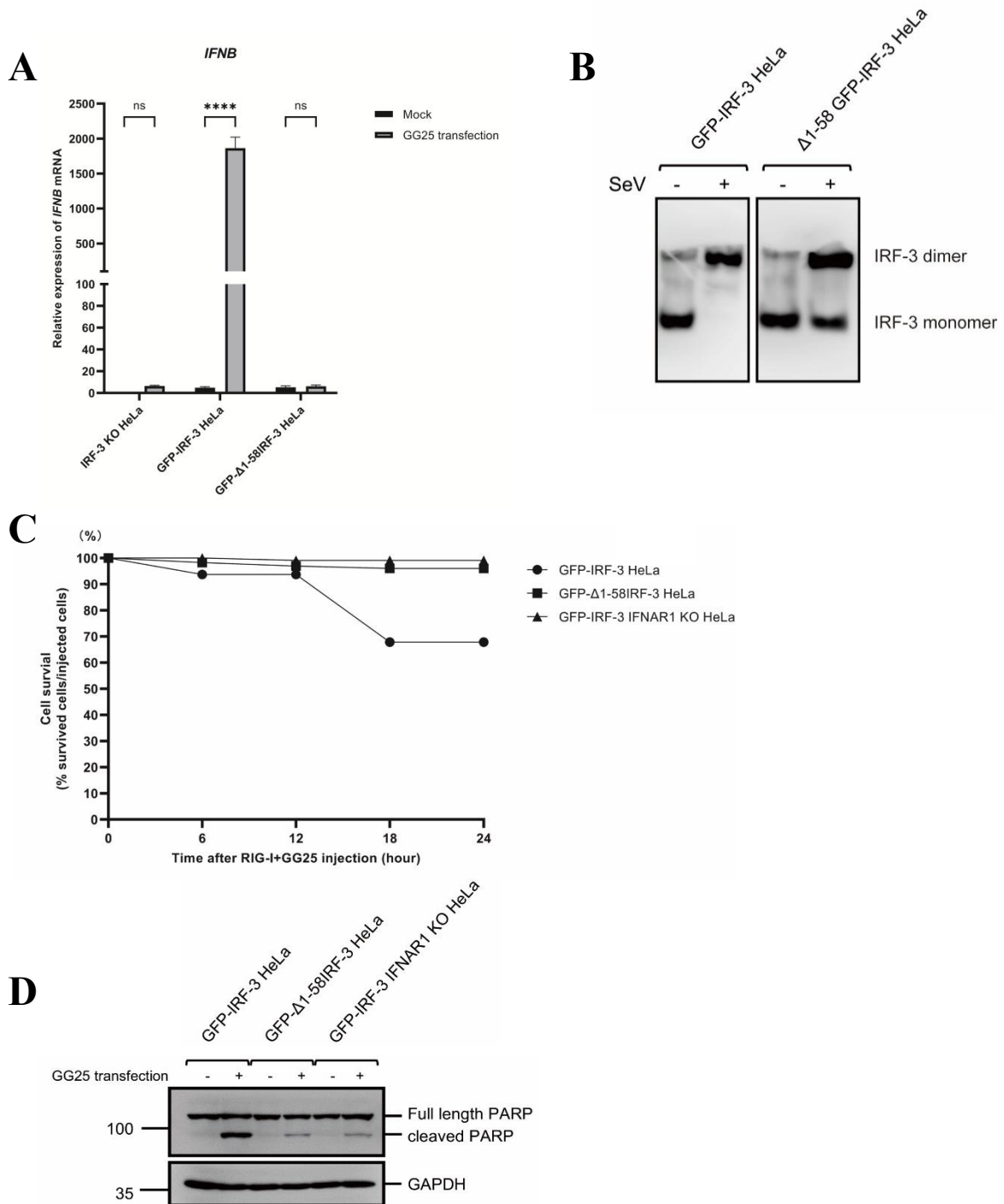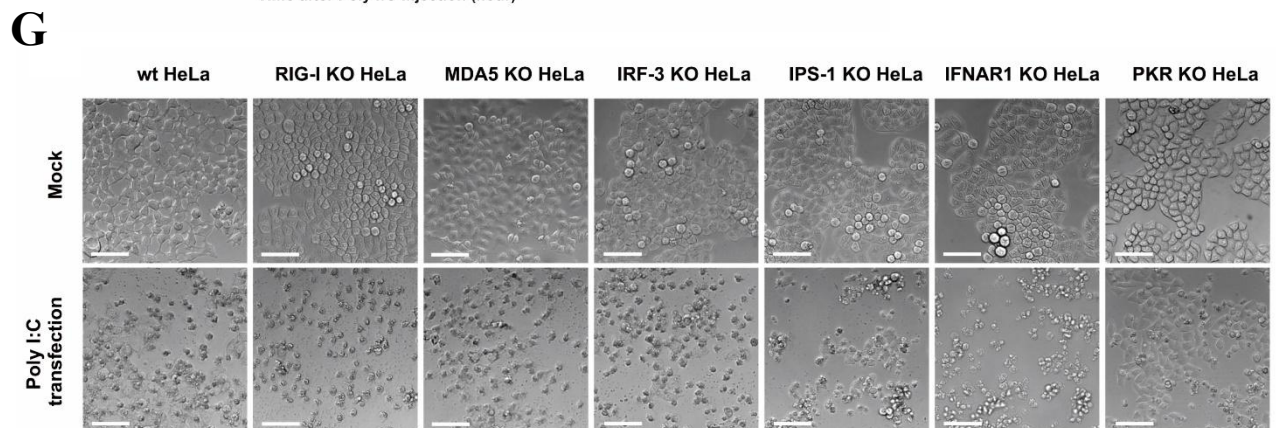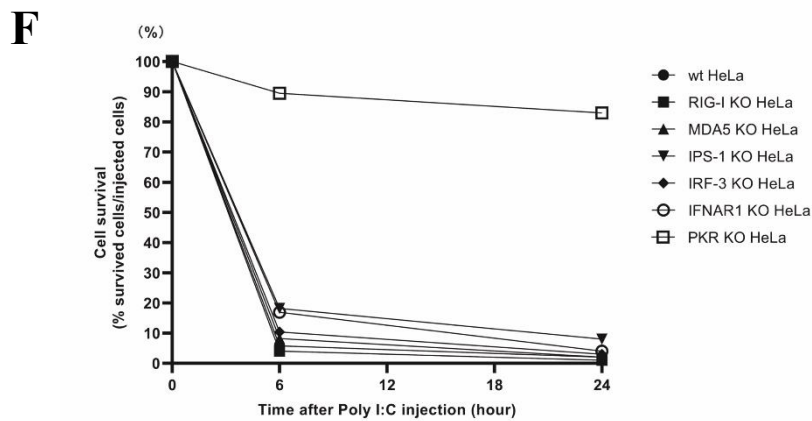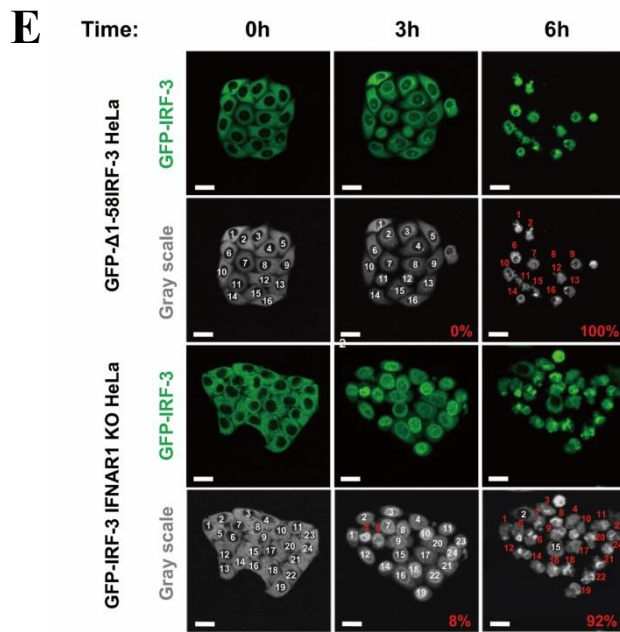
Figure 3. Diverse mechanisms of cell death induced by GG25 and poly I:C.

A: GFP-Δ1-58IRF-3 stable expressing HeLa cells upon GG25 transfection (4 μg/ml, 12 h) was examined by RT-qPCR. The means + SEM of three independent experiments are shown; data were analyzed by a two-way ANOVA followed by Tukey's multiple comparisons test; ****$P < 0.0001$; ns, not significant.

B: The dimerization of GFP-IRF-3 and GFP-Δ1-58IRF-3 was confirmed by native-PAGE and immunoblotting upon SeV infection (12 h). The relative expression of the *IFNB* gene in GFP-IRF-3 and

C: GFP-IRF-3 HeLa, GFP-Δ1-58IRF-3 HeLa, and GFP-IRF-3 IFNAR1 KO HeLa cells were injected with RIG-I and GG25 (1 μg/μl each), observed live for cell death, and quantified for % cell survival at the indicated time points.

D: The levels of cleaved PARP in GFP-IRF-3, GFP-Δ1-58IRF-3, and GFP-IRF-3 IFNAR1 KO HeLa cells upon the transfection of GG25 (4 μg/ml, 24 h) were examined by immunoblotting.
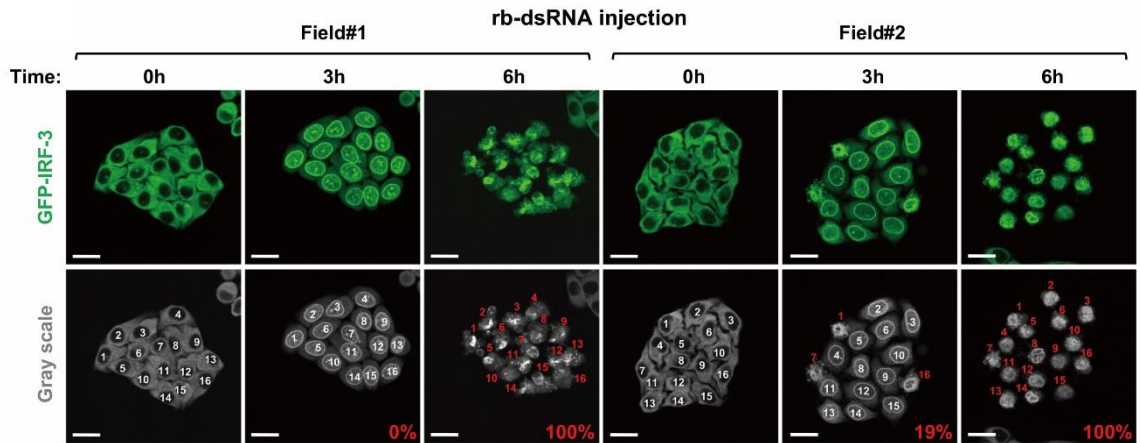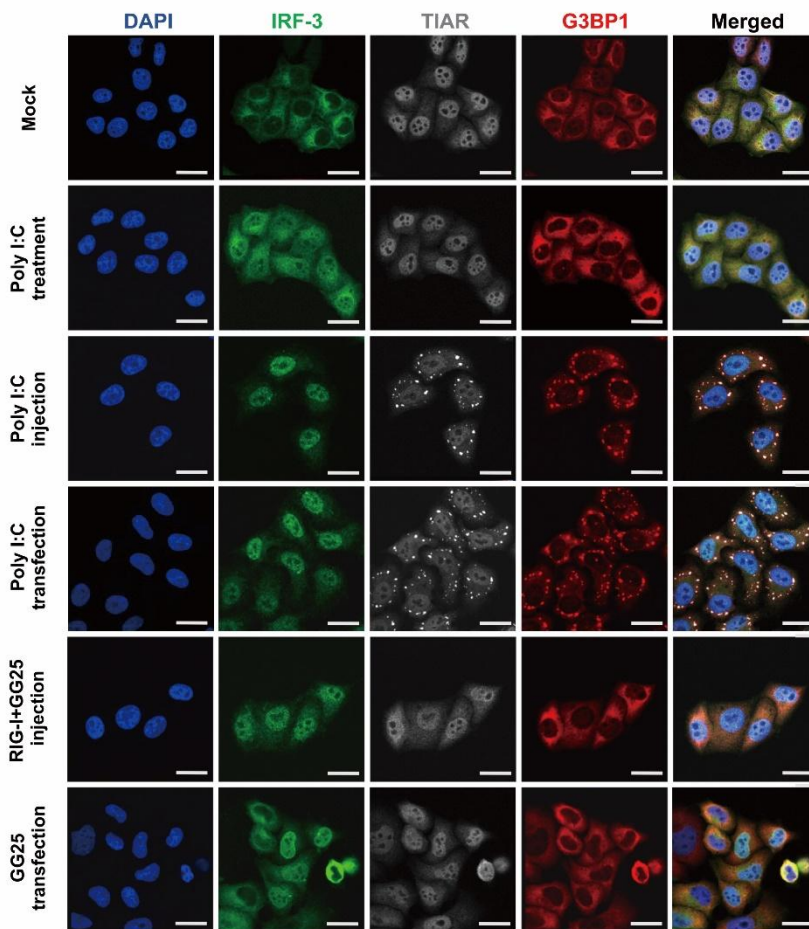
Figure 3. Diverse mechanisms of cell death induced by GG25 and poly I:C.

E: GFP-Δ1-58IRF-3 and GFP-IRF-3 IFNAR1 KO HeLa cells were injected with poly I:C (1 µg/µl) and observed live for the localization of IRF-3 and cell death at the indicated times after the injection. % Cell death was calculated and shown in red.

F: HeLa cells and indicated KO HeLa cells were injected with poly I:C (1 µg/µl), observed for cell death, and % cell survival was quantified.

G: Wild-type and the indicated KO HeLa cells were transfected with poly I:C (0.5 µg/ml, 24 h) and observed for cell death. Scale bar = 25 µm in (E) and 100 µm in (F).

**Figure 3. Diverse mechanisms of cell death induced by GG25 and poly I:C.**

H: GFP-IRF-3 HeLa cells were injected with rb-dsRNA (1 μg/μl) and observed live for the localization of IRF-3 and cell death at the indicated times after the injection. % Cell death was calculated and shown in red. Scale bar = 25 μm

I: GFP-IRF-3 HeLa cells were mock treated, treated with poly I:C (5 μg/ml in culture medium for 3 h), injected with poly I:C (1 μg/μl for 3 h), transfected with poly I:C (0.5 μg/ml in culture medium with lipofectamine for 3 h), injected with RIG-I and GG25 (1 μg/μl each for 3 h), or transfected with GG25 (4 μg/ml in culture medium with lipofectamine for 3 h). Cells were fixed and stained for TIAR and G3BP1 with respective antibodies for microscopy. Scale bar = 25 μm

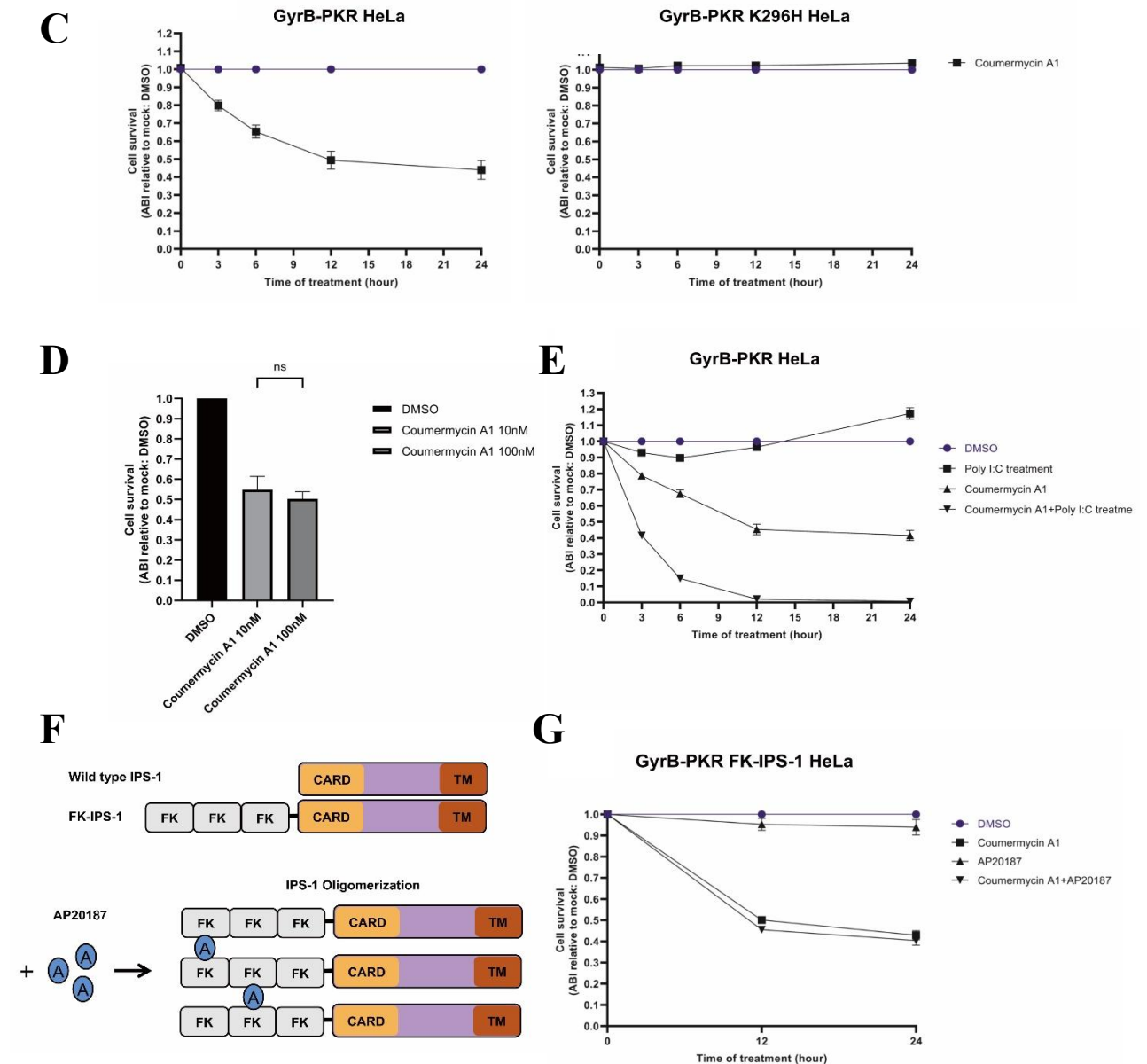## 3.4   Synergistic induction of cell death by PKR and poly I:C treatment.

It was noteworthy that cytosolic dsRNA strongly triggered apoptosis in a PKR-dependent and RLR-independent way. To further elucidate the role of PKR, a GyrB-PKR system is constructed, in which PKR activation is inducible by a small chemical, coumermycin A1 (Figure. 4A) (Friedrich et al., 2005; Ung et al., 2001). The dsRNA-binding domain of PKR was replaced by the bacterial Gyrase B subunit, and under the stimulation of coumermycin A1, the GyrB subunit dimerized and further induced PKR activation (Figure. 4A). Fusion protein GyrB-PKR or GyrB-PKR K296H (lacking kinase activity) were expressed in PKR KO HeLa cells to examine the consequence of sole activation of PKR in the absence of dsRNA (Figure. 4B; Figure. S3B). Coumermycin A1 induced PKR activation was confirmed by the formation of SG in GyrB-PKR HeLa, but not in GyrB-PKR K296H or PKR KO HeLa cells (Figure. 4C). Quantitative analysis of cell survival revealed that significant cell death was induced by sole activation of PKR by coumermycin A1; however, it appeared to be less prominent (45%) than that induced by injection of poly I:C (>95%) (Figure. 3F). Coumermycin A1 at higher concentration (100 nM) did not stimulate additional cell death (Figure. 4D). This result indicated that a combined activation of PKR and other dsRNA receptors may exert synergistic effects on the induction of cell death. Exogenous treatment of poly I:C, which activates TLR3 in endosomes, but not cytosolic PKR (Figure. 3I) was did not induce notable cell death over time. However combined treatment of poly I:C and coumermycin A1 induced almost complete cell death within 12 h (Figure. 4E).   Meanwhile to analyze the effect of IPS-1 on PKR dependent cell death, a FKBP fusion system was further incorporated into GyrB-PKR HeLa cells, by which, selectively activation of RLR signaling can be achieved by treatment of AP20187 (Figure 4F) (Takamatsu et al., 2013) . GyrB-PKR HeLa cells expressing FK-IPS-1 were treated with coumermycin A1, AP20187, or their combination (Figure. 4G). Activation of IPS-1 and PKR were confirmed by efficient nuclear translocation of IRF-3 and the induction of SG respectively under AP20187 and coumermycin treatment (Data not shown). However no significant synergistic effect of PKR and IPS-1 was observed (Figure. 4G).
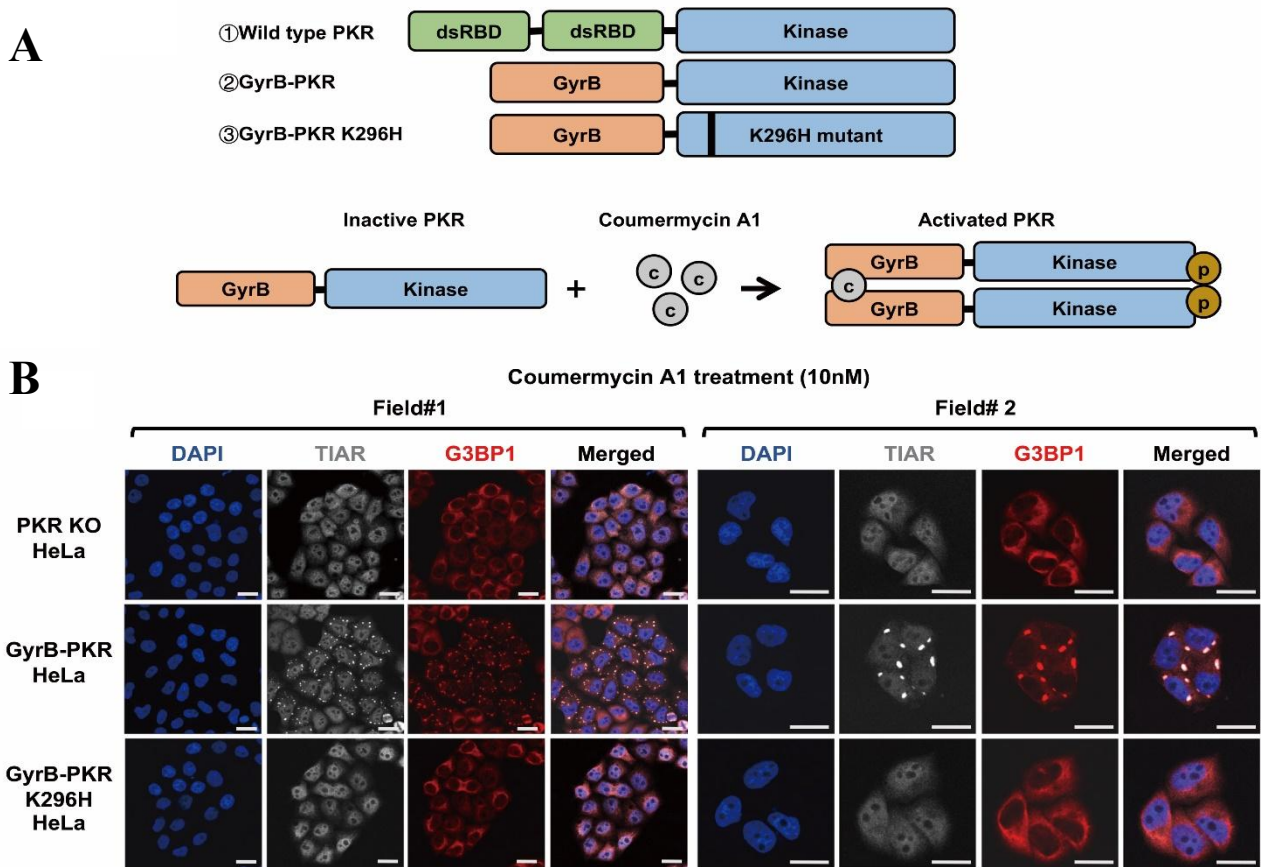
Figure 4. Synergistic induction of cell death by PKR and the exogenous poly I:C treatment.

A: Schematic representation of PKR and GyrB-PKR fusion proteins and the activation mechanism of GyrB-PKR fusion by coumermycin A1.

B: Induction of SG by the coumermycin A1 treatment. PKR KO HeLa, GyrB-PKR HeLa, and GyrB-PKR K296H HeLa cells were treated with coumermycin A1 (10 nM for 3 h) and observed for the SG marker TIAR (gray) and G3BP1 (red), as in Figure. 3I. Scale bar = 25 μm.

Figure 4. Synergistic induction of cell death by PKR and the exogenous poly I:C treatment.

C: GyrB-PKR HeLa and GyrB-PKR K296H HeLa cells were mock treated (DMSO) or treated with coumermycin A1 (10 nM) for the indicated times and examined for cell survival.

D: GyrB-PKR HeLa cells were mock treated (DMSO) or treated with coumermycin A1 at the indicated concentration for 12 h and then examined for cell survival.

E: GyrB-PKR HeLa cells were treated with the indicated chemicals and examined for cell survival at each time point.

F: Schematic representation of the IPS-1 and FK-IPS-1 fusion protein and activation mechanism.

G: GyrB-PKR FK-IPS-1 HeLa cells were treated with the indicated chemicals and examined for cell survival at each time point. Cell survival in (C), (D), (E), (G) was examined by the Amido black assay (Methods) and presented as Amido black intensity (ABI) relative to the mock. Data are represented as the means ± SEM of three independent experiments.

3.5   Involvement of TLR3 signaling in cell death induced by cytoplasmic poly I:C.

The combined treatment of coumermycin A1 and poly I:C resulted in robust cell death, however whether poly I:C injection practically triggers cell death via PKR and TLR3 signaling remains unclear. During injection, no IRF-3 translocation was observed in surrounding un-injected cells, indicating that, no extracellular leakage of poly I:C was significantly produced. Therefore, I hypothesized that the cytosolic injected poly I:C could also activate endosomal TLR3 in cytosol. Chloroquine and NH_4Cl were used to inhibit endosomal acidification, which is essential for dsRNA dependent activation of TLR3 (Hart & Young, 1991; Kuznik et al., 2011). These chemicals were shown to attenuate cell death induced by poly I:C injection (Figure. 5A). GyrB-PKR HeLa cells with TRIF KO (GyrB-PKR TRIF KO HeLa) were generated and stimulated with coumermycin A1, poly I:C or both to study the effect of TRIF, the adaptor protein of TLR3, in poly I:C mediated apoptotic signaling (Figure. 5B). Synergistic cell death induced by combined treatment of coumermycin A1 and poly I:C was not observed in GyrB-PKR TRIF KO HeLa cells, suggesting the involvement of TRIF in the process of cell death. Next injection of poly I:C were carried out in wild type, PKR KO, TRIF KO, and PKR/TRIF double KO (DKO) HeLa cells (Figure. S3C). Prominent cell death induced in wild-type HeLa cells was partially blocked by the deletion of TRIF, and full inhibited in DKO cells (Figure 5C). Transfection of poly I:C yield similar result in these cells (Figure. 5D). Notably TRIF and PKR KO did not affect the activation of each other based on the nuclear translocation of IRF-3 and the formation of SG (Figure 5E). These results are consistent with my hypothesis that the robust apoptotic cell death induced by cytoplasmic poly I:C was activated by PKR and endosomal TLR3/TRIF signaling.
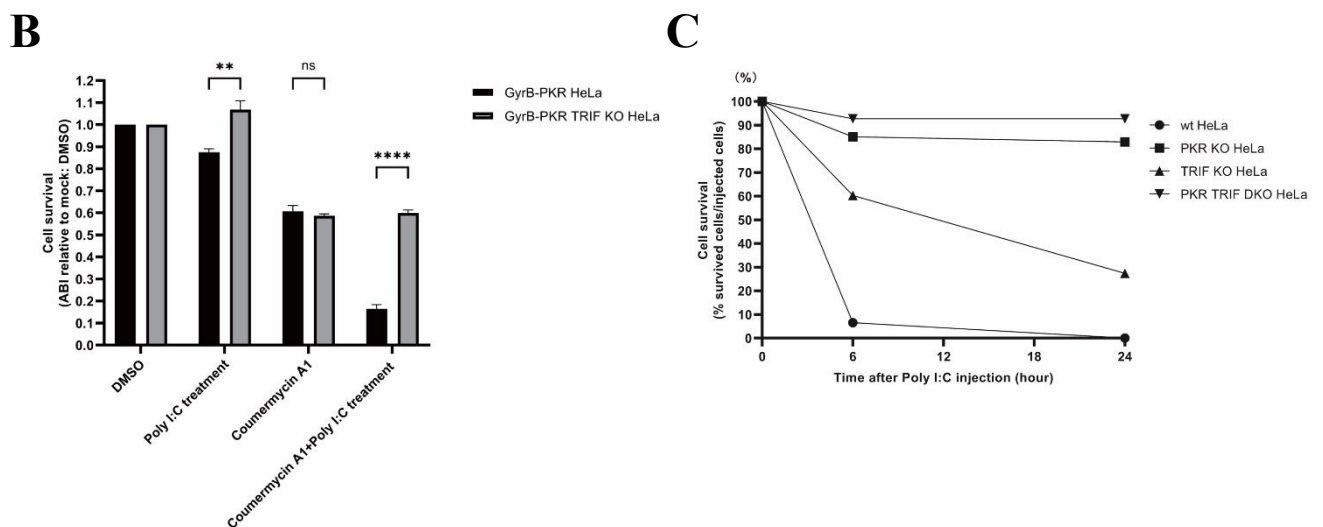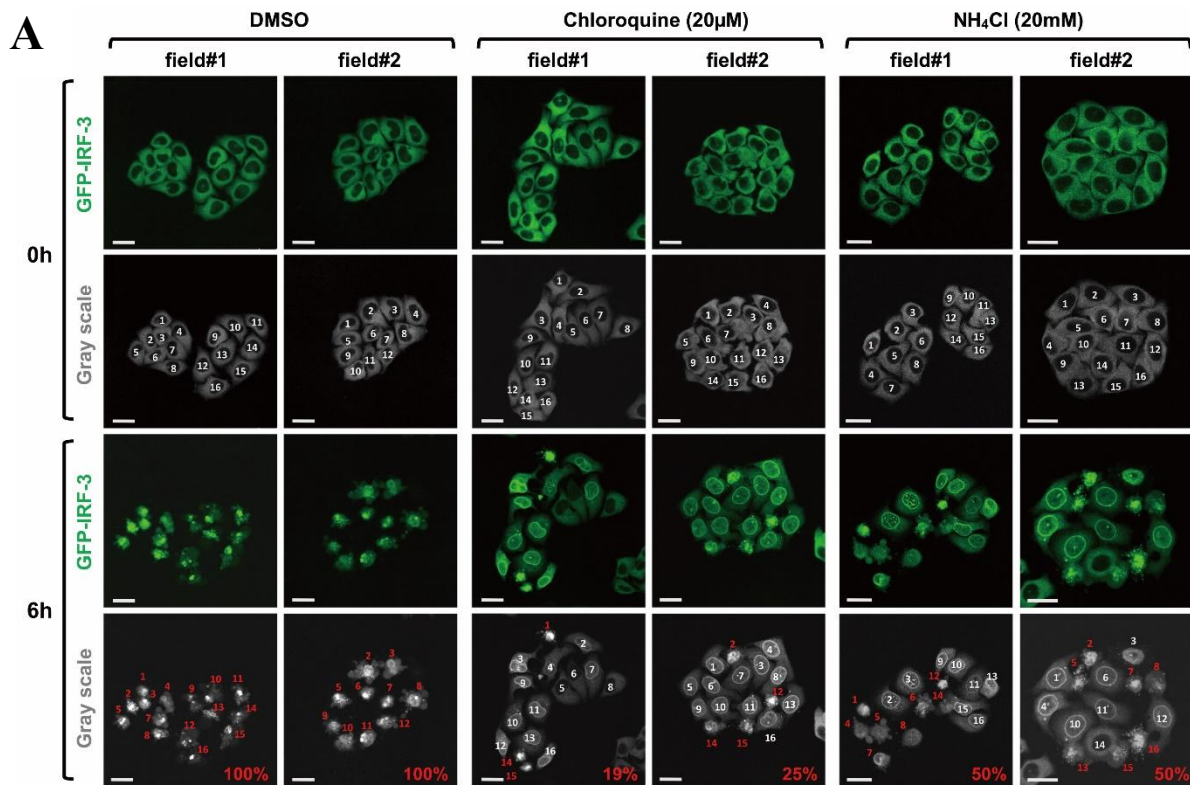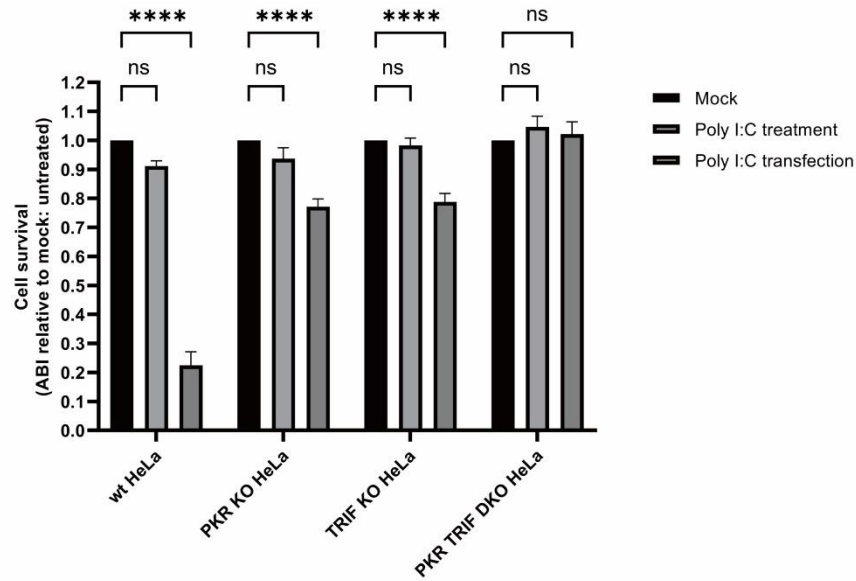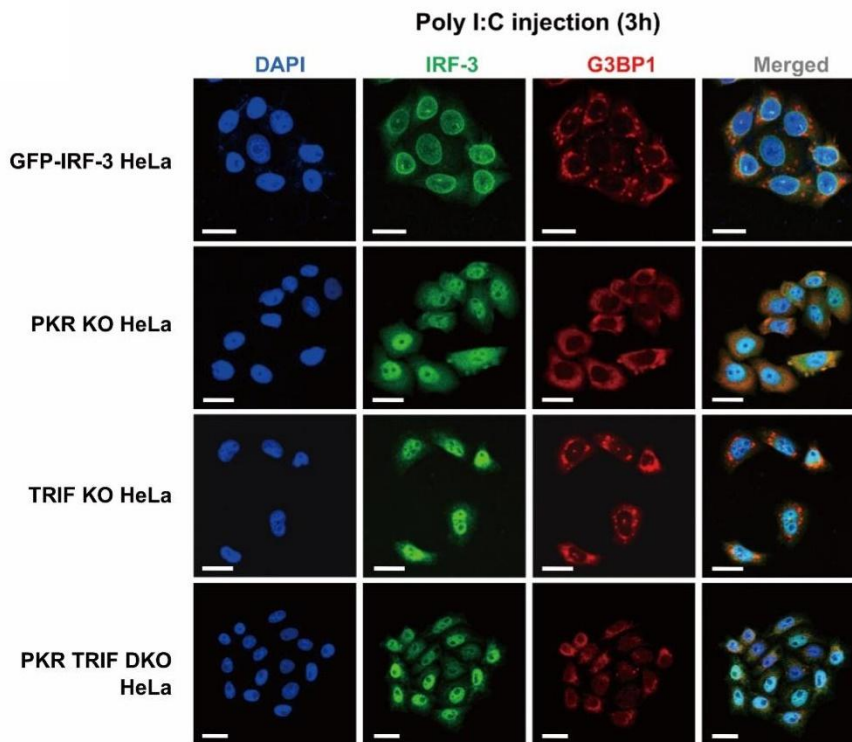
Figure 5. Involvement of TLR3 signaling in cell death induced by cytoplasmic poly I:C.

A: GFP-IRF-3 HeLa cells were treated with DMSO, chloroquine (20 μM for 6 h), or NH₄Cl (20 mM for 6 h) and then injected with poly I:C (1 μg/μl). GFP images of live cells were taken 0 and 6 h after the poly I:C injection. In each field, cells were numbered, assessed as dead (red) or alive (white), and % cell death was calculated. Scale bar = 25 μm.

B: GyrB-PKR HeLa and GyrB-PKR TRIF KO HeLa cells were treated with the indicated chemicals for 6 h and examined for cell survival. The means ± SEM of three independent experiments are shown; data were analyzed by a two-way ANOVA followed by Tukey's multiple comparisons test; **P <0.01, ****P < 0.0001; ns, not significant.

C: Wild-type, PKR KO, TRIF KO, and PKR TRIF DKO HeLa cells were injected with poly I:C (1 μg/μl), observed live for cell death, and % cell survival at the indicated time points was quantified.

Figure 5. Involvement of TLR3 signaling in cell death induced by cytoplasmic poly I:C.

D: Wild-type and the indicated KO HeLa cells were left untreated (Mock) or treated with poly I:C (5 μg/ml, 24 h) or transfected with poly I:C (0.5 μg/ml, 24 h), and were then examined for cell survival. The means + SEM of three independent experiments are shown; data were analyzed by a two-way ANOVA followed by Tukey's multiple comparisons test; ***$P < 0.001$, ****$P < 0.0001$; ns, not significant.

E: GFP-IRF-3, PKR KO, TRIF KO, and PKR TRIF DKO HeLa cells were injected with poly I:C (1 μg/μl) for 3 h, and then fixed and stained for IRF-3 (except GFP-IRF-3 HeLa cells) and G3BP1 with the respective antibodies for microscopy. Scale bar = 25 μm.

3.6 PKR activation led to decreased cFLIP which promoted endosomal TLR3 induced activation of caspases 8 and 9.

Previous studies suggested that activation of TLR3 triggered direct signaling of TRIF-FADD-caspase 8 cascade of apoptosis in certain types of cells (Alkurdi et al., 2018; McAllister et al., 2013; Salaun et al., 2006) . However, cFLIP, a FADD-like inhibitory protein was shown to inhibit FADD-caspase 8 signaling complex (DISC) by forming heterodimers with pro-caspase 8 (Safa, 2012; Tsuchiya et al., 2015). cFLIP is often highly expressed in cancer cells and is sensitive to cycloheximide (CHX) treatment (Alkurdi et al., 2018; Kreuz et al., 2001), indicating that cFLIP is a short half-life protein. The activation of PKR and downstream eIF2α was shown to inhibit translation initiation and halt *de novo* protein synthesis (Samuel, 1993). Thereby I hypothesized that the activation of PKR may result in the down-regulation of cFLIP which may promote caspase 8 activation and cell death.

To confirm this, GyrB-PKR HeLa cells were treated with coumermycin A1 and examined for cFLIP levels (Figure. 6A). As expected, markedly decreased cFLIP levels was detected after PKR activation, particularly those of the cFLIP S isoform. The effects of exogenous poly I:C treatment on cFLIP levels were next examined (Figure. 6B). No dramatic decrease of cFLIP L during 12 h of poly I:C treatment was observed. In contrast, cFLIP S levels raised, and the induction of cFLIP mRNA expression was also detected upon treatment of poly I:C (Figure. 6C). Cells treated with coumermycin A1, CHX, or poly I:C yield partially cleaved apoptosis markers, PARP, caspase 8, and caspase 9 (Figure. 6D). However, when exogenous poly I:C was treated combined with coumermycin A1 or CHX, the cleavage of apoptosis markers was markedly accelerated (Figure. 6D). The induction of cFLIP/S by the poly I:C treatment was abrogated by the co-treatment with coumermycin A1 or CHX. These results indicate the importance of cFLIP levels in the regulation of cell death. To analyze the role of cFLIP in cell death regulated by PKR and TRIF, cFLIP levels were manipulated by siRNA and overexpression. PKR activation induced cell death was weakly promoted by the knockdown of cFLIP (Figure. 6E). The stimulation of TLR3 alone again did not induce notable cell death; however, cell death was largely promoted in cells with knockdown of cFLIP. Co-activation of PKR and TLR3 induced robust cell death, which did not further

promote cell death by knockdown of cFLIP. Next the effects of cFLIP overexpression were examined (Figure. 6F). cFLIP overexpression significantly prevented cell death triggered by different stimuli. PKR activation induced cell death was partially attenuated by the overexpression of cFLIP, but not fully recovered to non-stimulated level. The prominent cell death induced by the co-activation of PKR and TLR3 was significantly suppressed by the overexpression of cFLIP, even though, incompletely. These results indicated that cell death induced by PKR was, at least in part, promoted by down-regulation of cFLIP, as PKR has also been reported to induce cell death directly through the mitochondrial pathway way (García et al., 2007; Gil et al., 2002) . The roles of PKR and TLR3 in the regulation of cFLIP and further activation of apoptotic signals were confirmed by the transfection of poly I:C in wild-type, PKR KO, TRIF KO and DKO HeLa cells (Figure. 6G). In cells lacking PKR (PKR KO and DKO), the down-regulation of cFLIP L/S was not observed, and the production of apoptotic markers including cleaved PARP, caspases 8 and 9 was partially decreased in single KO HeLa cells (PKR KO and TRIF KO) and completely abolished in DKO HeLa cells. In comparison with injection experiment, transfection of poly I:C in HeLa cells delayed the onset of apoptosis (Figure. 6H). Nevertheless, in cells under poly I:C transfection, the levels of apoptotic markers produced (Figure. 6G) were consistent with the degree of cell death observed (Figure. 6I).
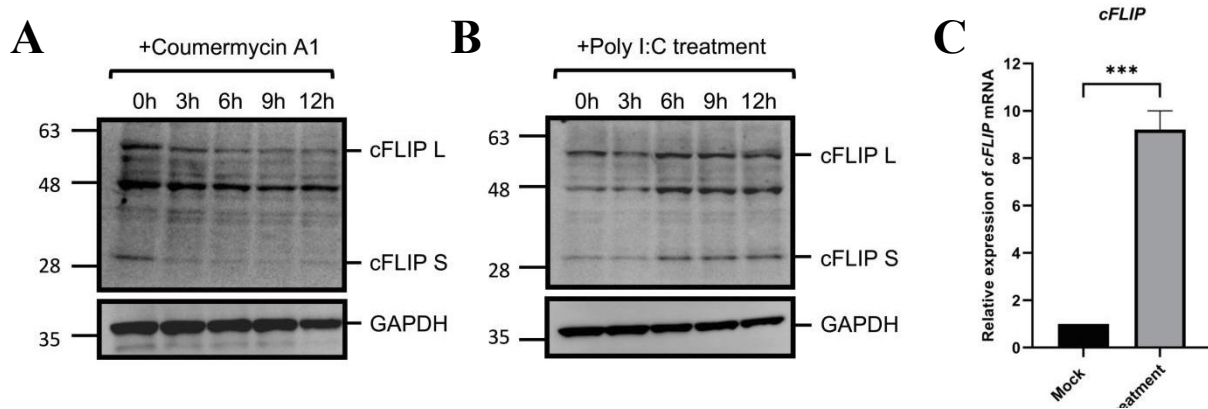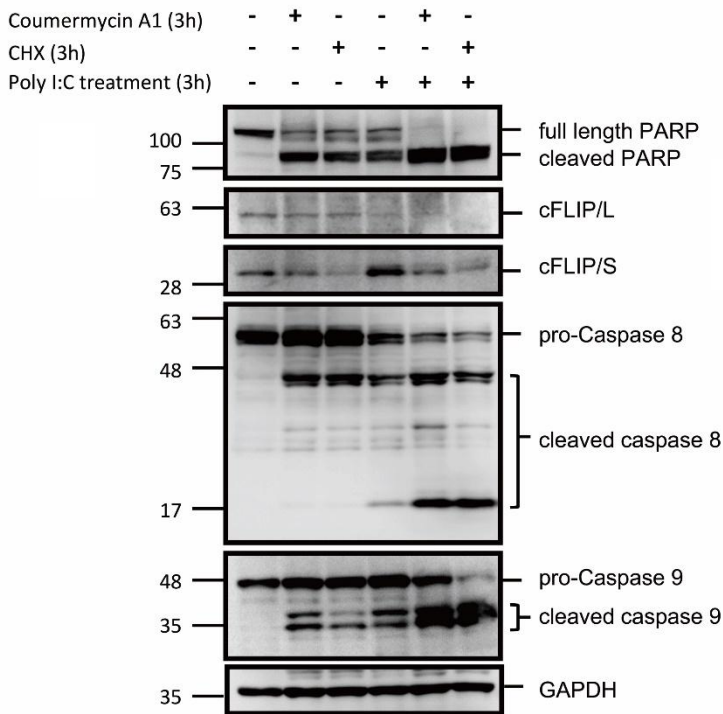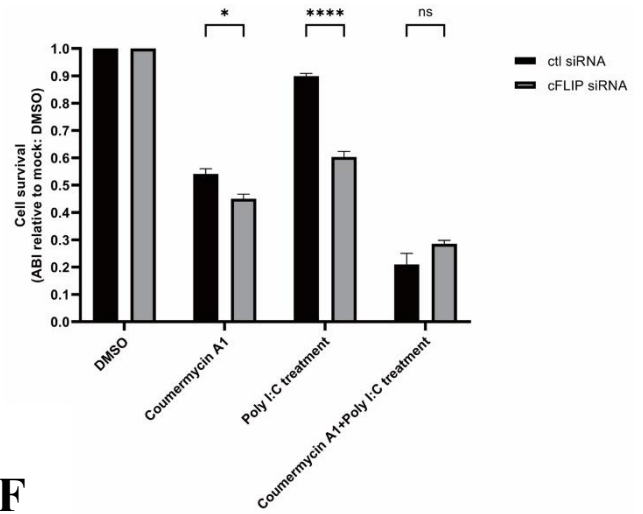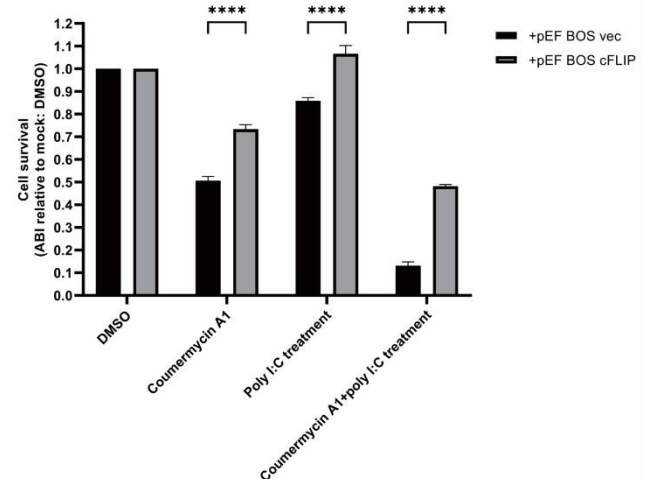
Figure 6. PKR activation resulted in the down-regulation of cFLIP and promoted the endosomal TLR3-induced activation of caspases 8 and 9.

A: GyrB-PKR HeLa cells were treated with coumermycin A1 for the indicated times and examined for the levels of cFLIP L, cFLIP S, and GAPDH by immunoblotting.

B: GyrB-PKR HeLa cells were treated with poly I:C (5 µg/ml) and examined for the levels of cFLIP L, cFLIP S, and GAPDH by immunoblotting.

C: GyrB-PKR HeLa cells were left untreated or treated with poly I:C (5 µg/ml, 6 h). Cells were harvested and the relative expression of the *cFLIP* gene was examined by RT-qPCR. The means + SEM of three independent experiments are shown; data were analyzed by an unpaired *t*-test; ***$P < 0.001$.
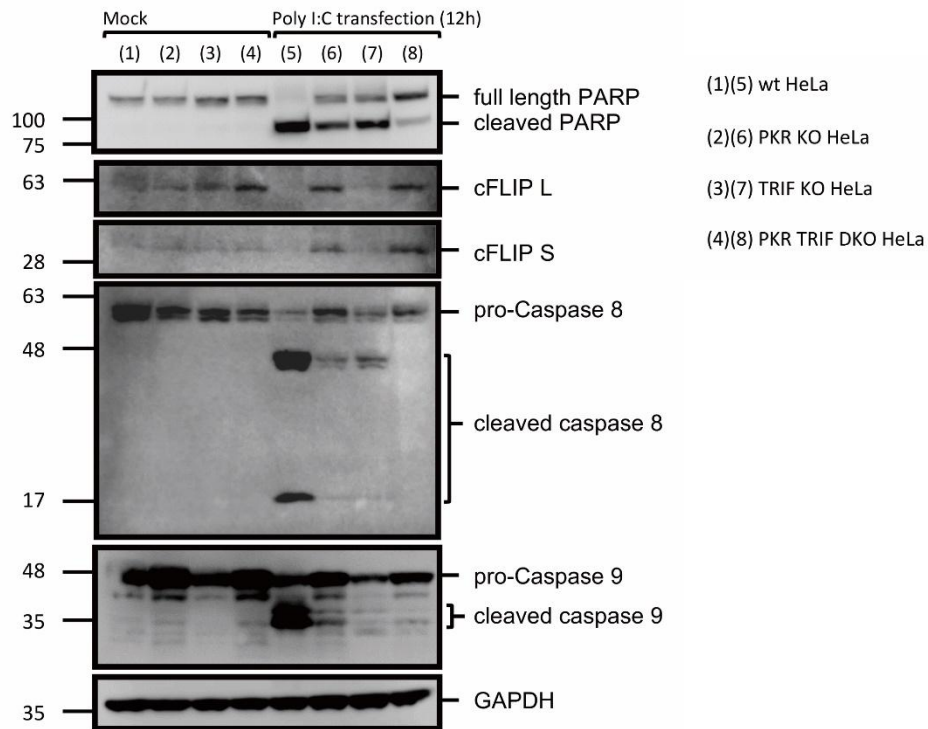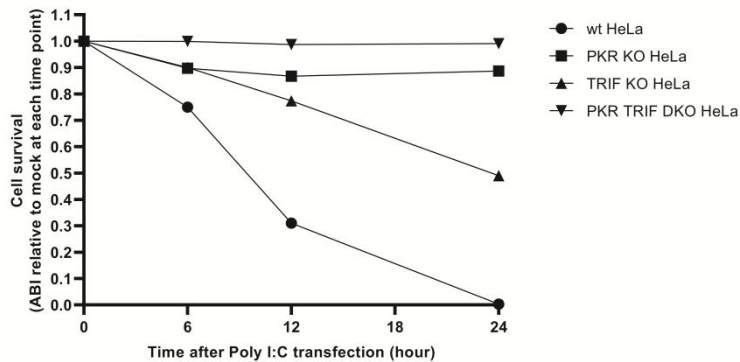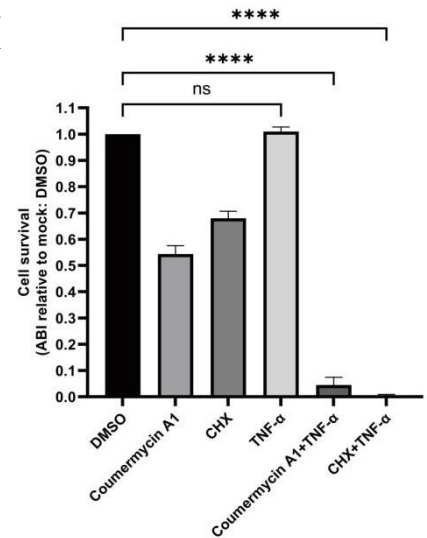
D

Coumermycin A1 (3h)	-	+	-	-	+	-
CHX (3h)	-	-	+	-	-	+
Poly I:C treatment (3h)	-	-	-	+	+	+

100 — full length PARP
75 — cleaved PARP

63 — cFLIP/L

28 — cFLIP/S

63 — pro-Caspase 8
48 —

cleaved caspase 8

17 —

48 — pro-Caspase 9
35 — cleaved caspase 9

35 — GAPDH

E

Cell survival (ABI relative to mock: DMSO)

- ctl siRNA
- cFLIP siRNA

DMSO / Coumermycin A1 (*) / Poly I:C treatment (****) / Coumermycin A1+Poly I:C treatment (ns)

F

Cell survival (ABI relative to mock: DMSO)

- +pEF BOS vec
- +pEF BOS cFLIP

DMSO / Coumermycin A1 (****) / Poly I:C treatment (****) / Coumermycin A1+poly I:C treatment (****)

Figure 6. PKR activation resulted in the down-regulation of cFLIP and promoted the endosomal TLR3-induced activation of caspases 8 and 9.

D: GyrB-PKR HeLa cells were treated with the indicated chemicals (10 nM coumermycin A1; 10 μg/ml CHX; 5 μg/ml poly I:C) for 3 h and examined for the indicated proteins by immunoblotting.

E: GyrB-PKR HeLa cells were transfected with control (ctl) or specific siRNA for cFLIP for 48 h, treated with the indicated chemicals as in (D), and examined for cell survival.

F: GyrB-PKR HeLa cells were transfected with the control (pEF BOS vec) or expression vector for cFLIP (pEF BOS cFLIP) for 48 h, treated with the indicated chemicals as in (D), and examined for cell survival. Cell survival in (E), (F) is presented as ABI relative to the mock, and the means ± SEM of three independent experiments are shown; data were analyzed by a two-way ANOVA followed by Tukey's multiple comparisons test; *P <0.05, ****P < 0.0001; ns, not significant. Refer to full-length Western blot images in supplemental materials.

G: Mock — (1) (2) (3) (4) | Poly I:C transfection (12h) — (5) (6) (7) (8)

full length PARP
cleaved PARP
cFLIP L
cFLIP S
pro-Caspase 8
cleaved caspase 8
pro-Caspase 9
cleaved caspase 9
GAPDH

(1)(5) wt HeLa
(2)(6) PKR KO HeLa
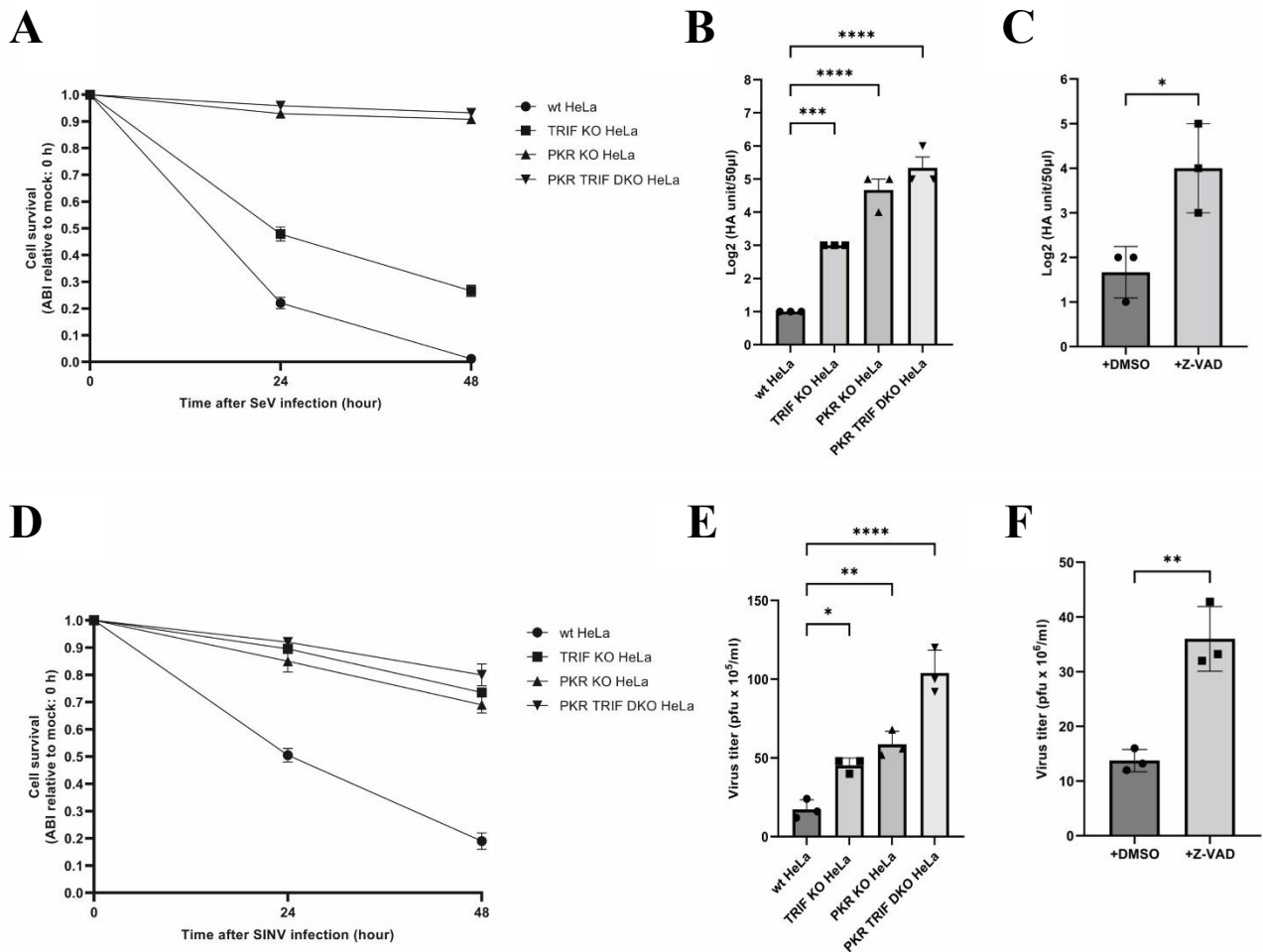(3)(7) TRIF KO HeLa
(4)(8) PKR TRIF DKO HeLa

Figure 6. PKR activation resulted in the down-regulation of cFLIP and promoted the endosomal TLR3-induced activation of caspases 8 and 9.

G: Wild-type, PKR KO, TRIF KO, and PKR TRIF DKO HeLa cells were transfected with poly I:C (0.5 µg/ml) for 12 h and examined for the indicated proteins by immunoblotting. **H**: Wild-type and the indicated HeLa cells were transfected with poly I:C (0.5 µg/ml) and examined for cell survival at the indicated time points.

I: GyrB-PKR HeLa cells were mock treated (DMSO) or treated with the indicated stimulant for 12 h and examined for cell survival. The means + SEM of three independent experiments are shown

51

3.7 Effect of PKR and TLR3/TRIF on virus-induced cell death and viral production.

dsRNA is not commonly produced in normal mammalian cells, but accidentally accumulates during viral replication. Sendai virus (SeV), a negative-sense single stranded RNA virus, produces massive dsRNA during infection. We, therefore, investigate the roles of PKR and TLR3/TRIF in SeV-induced cell death (Figure. 7A) and viral yield (Figure. 7B). SeV induced cell death was shown to be vigorous in wild-type HeLa cells, which is partially attenuated in HeLa cells with TRIF KO, and strongly inhibited in HeLa cells with PKR KO and DKO. Associated with the cell death inhibition, viral yield in culture medium markedly induced in PKR KO and DKO HeLa cells (Figure. 7B). More importantly, inhibiting cell death by Z-VAD treatment significantly increased viral production in wild-type HeLa cells (Figure. 7C). These results confirmed that the viral inhibition was directly induced by the onset of apoptosis. When Sindbis virus (SINV), a positive strand RNA virus, was examined, similar results were obtained (Figure. 7D, E, F). Signaling mediated by PKR and TLR3/TRIF significantly promoted virus-induced apoptosis and the inhibition of viral replication. A schematic view of the anti-viral apoptotic pathway induced by viral dsRNA is depicted in Figure. 8.

Figure 7. Roles of PKR and TLR3/TRIF in virus-induced cell death and viral yield.

A: Wild-type, PKR KO, TRIF KO, and PKR TRIF DKO HeLa cells were mock treated or infected with Sendai virus (SeV) for 48 h, and quantified for cell survival.

B: HA yield in the culture supernatant of cells infected in (A) were examined.

C: Wild-type HeLa cells were infected with SeV with or without Z-VAD (50 μM) in culture medium for 72 h, and the culture supernatant was examined for HA yield.

D: The same set of cells in (A) were mock treated or infected with Sindbis virus (SINV) for 48 h and quantified for cell survival.

E: Viral titers in the culture supernatant of cells in (D) were examined by a plaque assay.

F: Wild-type HeLa cells were infected with SINV with or without Z-VAD (50 μM) in culture medium for 72 h, and viral titers in the culture supernatant were examined by the plaque assay. The means ± SEM of three independent experiments are shown; data in (B) and (D) were analyzed by a one-way ANOVA followed by Dunnett's multiple comparisons test; data in (C) and (F) were analyzed by an unpaired t-test; $*P < 0.05$, $**P < 0.01$, $***P < 0.001$, $****P < 0.0001$.
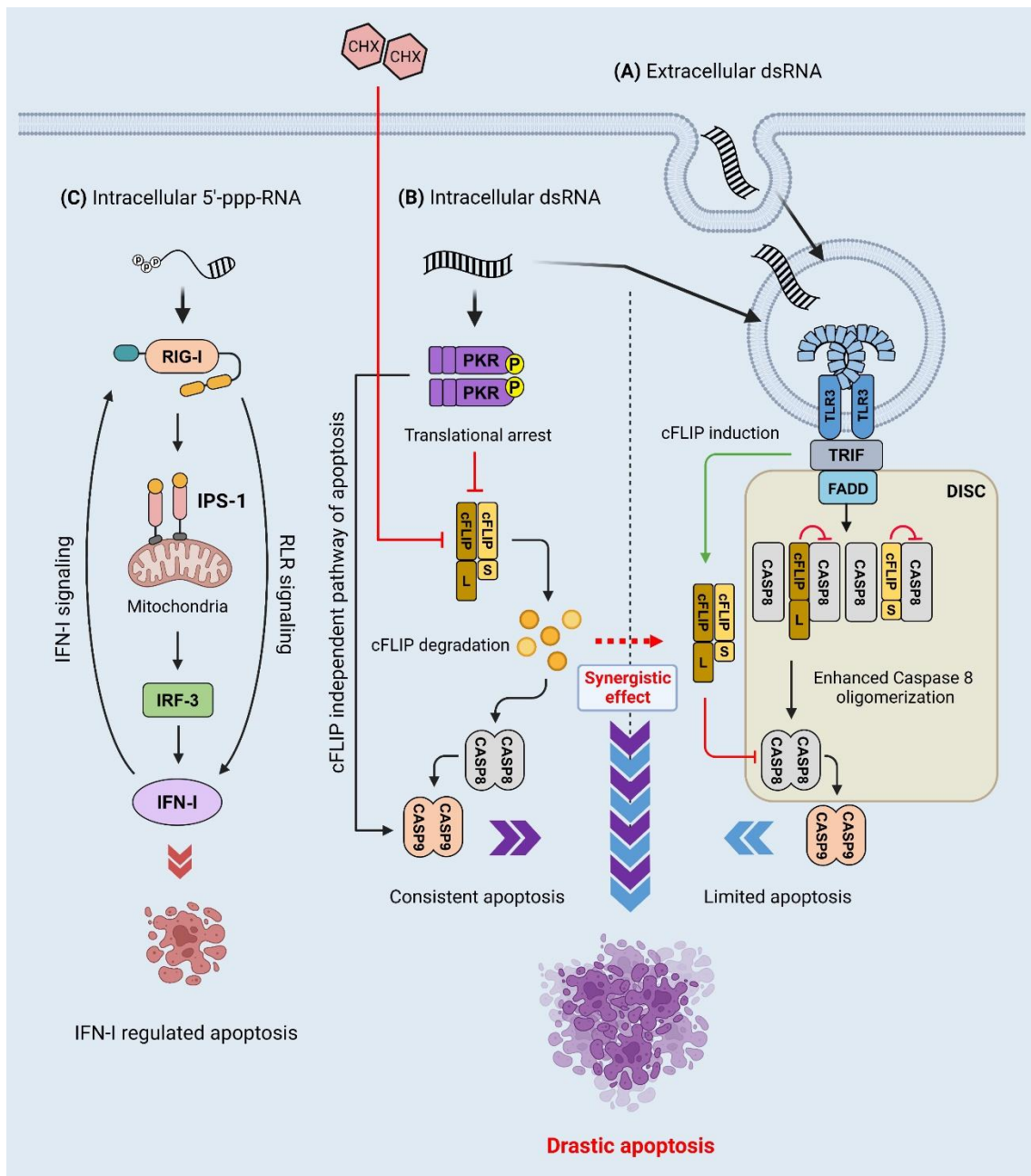
Figure 8. Schematic view of cell death signaling induced by extracellular dsRNA, intracellular dsRNA and 5'-ppp-RNA.

(A): Extracellular dsRNA is up taken by endocytosis and recognized by TLR3. TLR3 signals with TRIF to induce the production of IFN-I and at same time induce the expression of cFLIP to negatively regulate caspase 8. The TLR3 signaling complex also interact with FADD to activate the DISC-containing caspase 8, however apoptosis is inhibited by the induction of cFLIP. **(B):** Intracellular dsRNA delivered by the injection or transfection activates TLR3 through endosomal entrapment as above. In contrast to endosomal dsRNA, cytosolic dsRNA also activates PKR, which induces SG formation and translational arrest, leading to the down-regulation of cFLIP and apoptosis via the activation of caspase 8. In addition, PKR was also reported to promote the mitochondrial dependent pathway of apoptosis with caspase 9 activation; therefore, robust apoptosis was induced via caspases 8/9. **(C):** Intracellular short 5'-ppp-dsRNA is sensed by RIG-I, leading to the induction of IFN-I, and limited apoptosis was induced with slow kinetics. This apoptosis is regulated by IRF-3 and IFN-I. Figure 8 is created with BioRender.com.

A
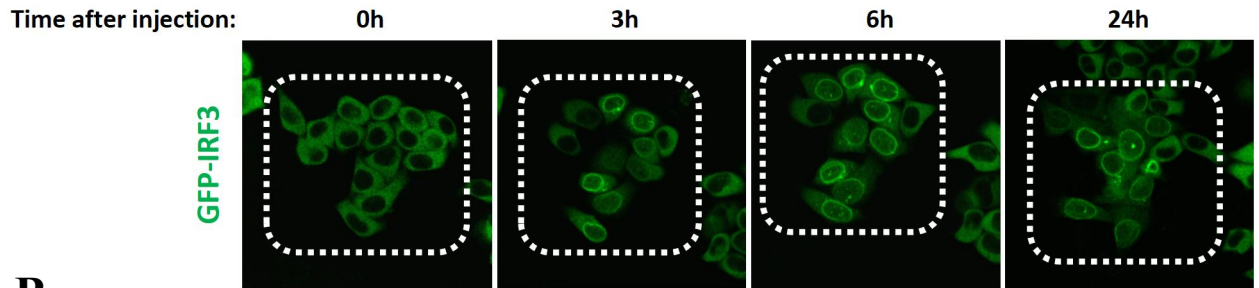
B
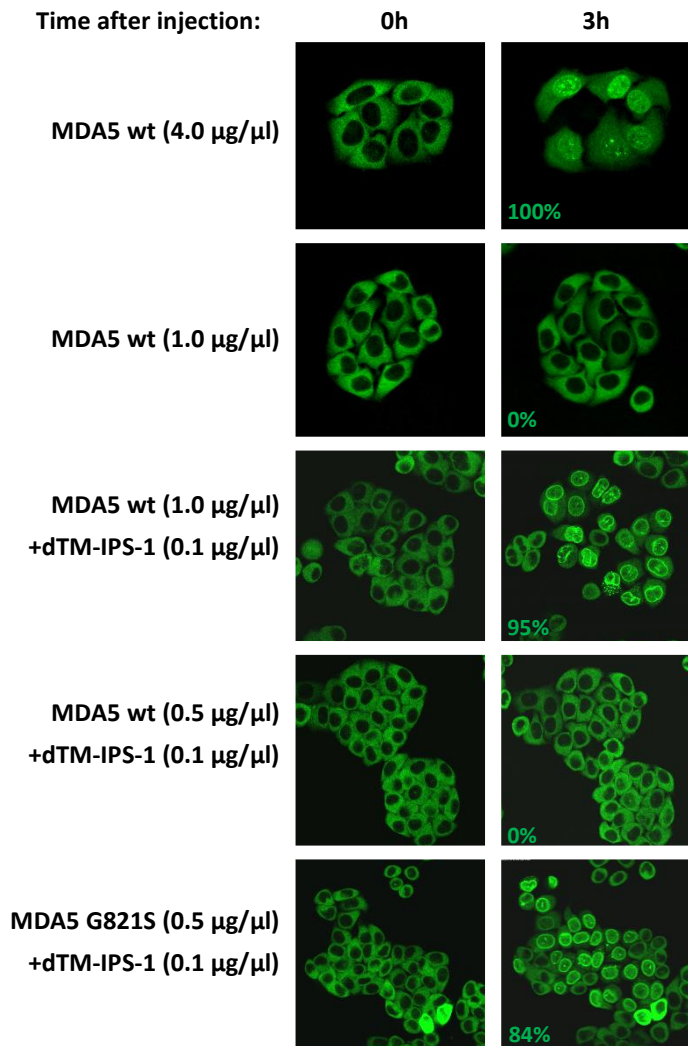
Figure S1. Supplementary data of injection and live cell imaging

A: GFP-IRF-3 HeLa cells were transfected with PKR siRNA for 48 h and injected with poly I:C (1.0 μg/μl), cells were imaged at indicated time points after injection. Injected cells were circled in dotted box

B: GFP-IRF-3 HeLa cells were injected with indicated substrates and imaged for IRF-3 localization. Percentage of cells that shown nuclear IRF-3 at 3 h after injection was calculated in green number.
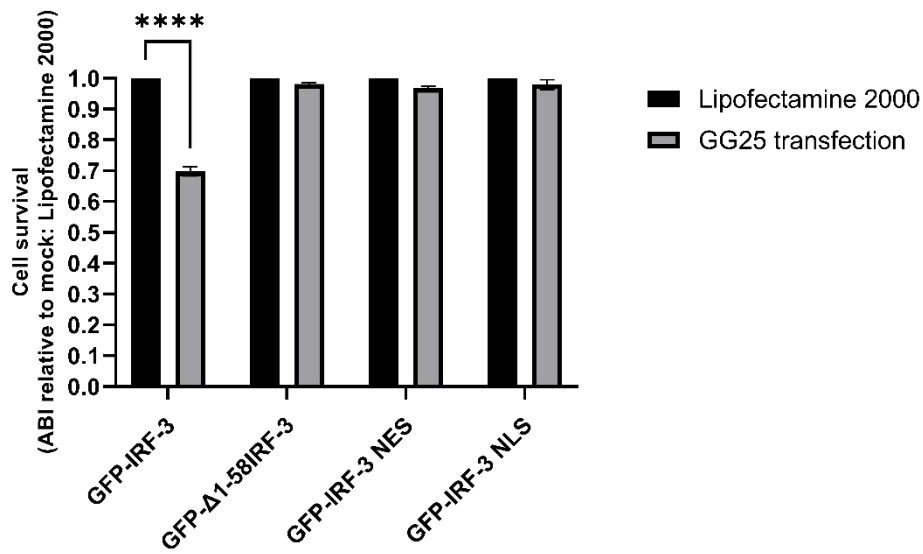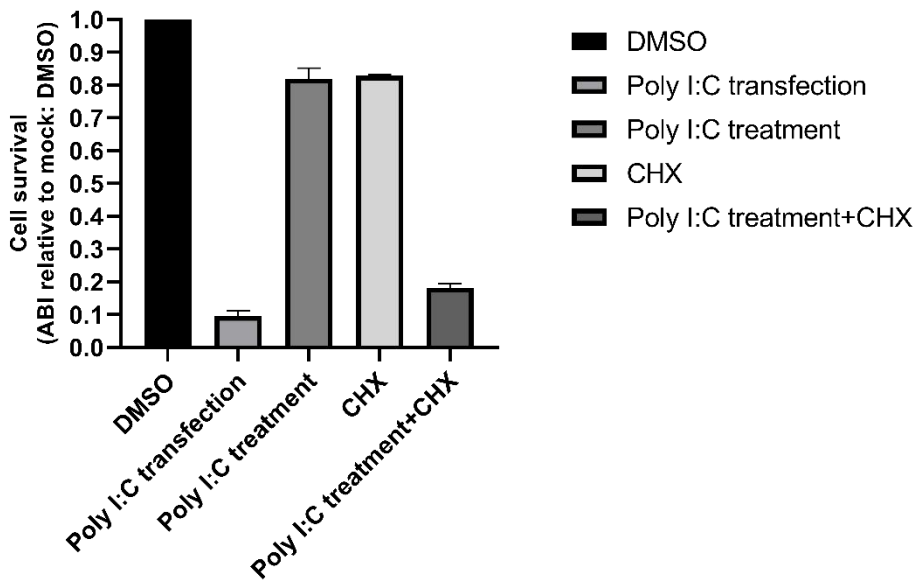
Figure S2. Supplementary data of cell survival quantification

A: IRF-3 KO HeLa cells expressing GFP-IRF-3, GFP-Δ1-58IRF-3, GFP-IRF-3 NES and GFP-IRF-3 NLS were transfected with lipofectamine 2000 only or lipofectamine 2000 with GG25 (4 μg/ml) for 24 h and quantified for cell survival.

B: HT1080 cells were transfected with poly I:C (0.5 μg/ml) or treated with DMSO, exogenous poly I:C (5 μg/ml), CHX (10 μg/ml) or both poly I:C and CHX for 24 h and quantified for cell survival.
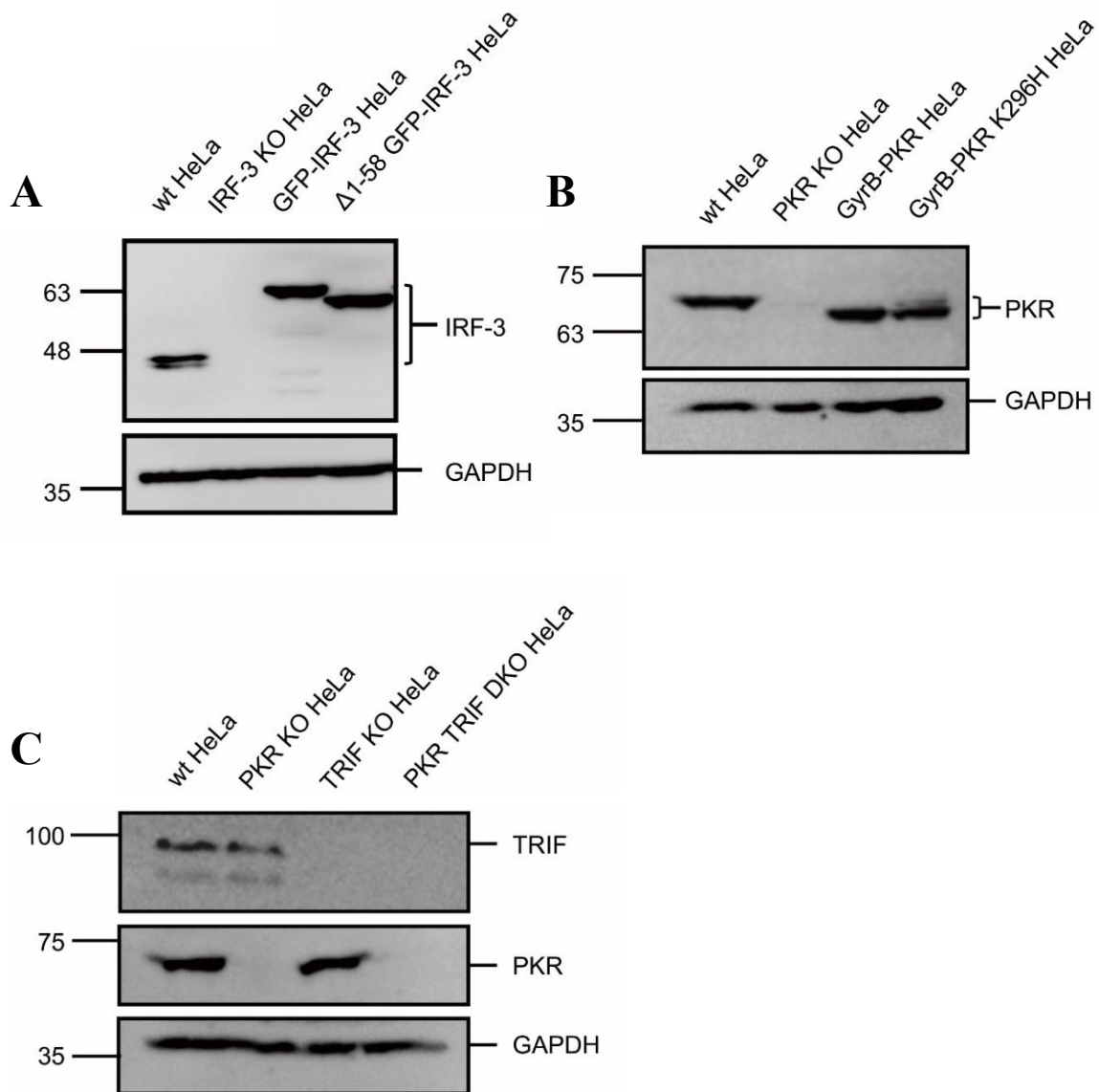
Figure S3. Supplementary data of knock out cell line confirmation

A: The expression of the GFP-IRF-3 and GFP-Δ1-58IRF-3 fusion protein in stably expressing HeLa cells was examined by immunoblotting.

B: The expression of the GyrB-PKR and GyrB-PKR K296H fusion protein in stably expressing HeLa cells was examined by immunoblotting.

C: The expression of PKR and TRIF in PKR KO, TRIF KO, and PKR TRIF DKO HeLa cells was examined by immunoblotting.

CHAPTER 4

DISCUSSION

DISCUSSION

Programmed cell death is strictly regulated by multiple mechanisms, and accidental discharge of cell death signal causes critical damage to the host cells. The current study investigated the mechanisms underlying cell death induced by intracellular dsRNA. A microinjection method was used to stimulate cells with cytoplasmic RNA without harming cell viability.

RIG-I, senses relatively short viral dsRNA in cytoplasm and induces the production of IFN-I. A short 5'-ppp dsRNA, GG25, is used to selectively activate RIG-I (Hornung et al., 2006; Pichlmair et al., 2006). The cytoplasmic injection of RIG-I+GG25 induced efficient IRF-3 nuclear translocation and subsequent IFN-I production (Figure. 1C). Among cells that shown nuclear IRF-3, no major cell death was observed within 12 h, and a fraction of cells (50-60%) underwent apoptosis 16 h after the injection (Figure. 2D). It is interesting to know that without IFN-I priming or RIG-I addition, GG25 exhibited low efficiency for IRF-3 activation, even though injected at high concentration (data not shown). This indicates that the level of endogenous RIG-I but not its ligand is essential for IRF-3 activation, therefore, emphasizing the importance of IFN-I feedback loop on RIG-I signaling.

The analyses further revealed that the IRF-3 transcriptional activity and IFN-I mediated secondary activation of genes were crucial for the induction of death signal by 5'-ppp-RNA (Figure. 3C). Not only for Δ1-58IRF-3, IRF-3 with deficiency in nuclear localization signal (NLS) and nuclear export signaling (NES), which do not trigger IFN-I production, also failed to induce cell death upon GG25 injection and transfection (Figure S2A). These results also suggested that the activation of RIG-I essentially activated IFN-I signaling but did not trigger direct cell death by itself (Figure. 8a). Which is consistent with previous study showing that OAS1/RNase L triggers apoptosis in response to RIG-I induced IFN-I production (Boehmer et al., 2021).

Similarly, cytoplasmic injected dsRNA mimic poly I:C triggered the robust nuclear translocation of IRF-3 (~100%) but strongly induced apoptotic cell death within 6 h (Figure. 1B, 2A). The base composition of poly I:C differed from that of viral dsRNA. To rule out

the possibility that the prominent cell death induced by poly I:C injection was caused by its base sequence, the natural rb-dsRNA was used to confirm the commonality of mechanism underlying cell death induced by the dsRNA. Efficient nuclear translocation of IRF-3 and rapid cell death were induced by rb-dsRNA, and cell death pattern were indistinguishable from that induced by poly I:C (Figure. 3H). Both transfection and exogenous treatments of poly I:C were commonly used to stimulate cells for IFN-I; however, the cell fates were markedly distinct (Figure. 5D), and the determination of this has not been clearly understood. Different from GG25, a sole ligand of RIG-I, cytoplasmic poly I:C fragments with various lengths, efficiently activate RIG-I and MDA5, and resulted in IFN-I production. However, by examining a serious of KO cells, RIG-I, MDA5 and their effector protein IPS-1 were shown to be dispensable for the apoptosis induced by cytosolic dsRNA, and PKR was further identified as an essential regulator of this cell death event (Figure. 3F, G). Consistent with the results obtained from PKR KO HeLa, PKR siRNA treatment in wild type HeLa significantly impaired poly I:C induced cell death (Figure S1A). PKR activation causes eIF2α phosphorylation and shut down of protein synthesis. PKR is well known for its ability to inhibit viral protein production under different infection cases. inhibit poly I:C Furthermore, artificial activation of re-constructed PKR by small molecule chemical without using dsRNA was demonstrated to induce notable cell death and the PKR kinase activity was shown to be essential (Figure. 4A, C). These data are consistent with previous findings showing that PKR triggers cell death signal via the mitochondrial components (García et al., 2007; Gil et al., 2002) . However, cell death promoted by sole activation of PKR was less efficient (~50%, Figure. 4C) than that induced by poly I:C injection (~100%, Figure. 3F), indicating the involvement of other signals that cooperated with PKR during cell death induction by poly I:C.

I speculated that endosomal TLR3 could detect cytoplasmic dsRNA as the third avenue for cell death induction. Poly I:C directly added to the culture medium was taken up by cells through endocytosis which activated endosomal TLR3. Nuclear translocation of IRF-3 was induced upon TLR3 activation (Figure. 3I), however, no prominent cell death was induced in HeLa cells over time (Figure. 4E). Interestingly, robust cell death was promoted by the co-stimulation of TLR3 and PKR (Figure. 4E). Knock out of TLR3 adaptor protein TRIF

attenuated the apoptosis induced by either TLR3 and PKR co-stimulation or the poly I:C injection (Figure 5B, C), suggesting that cytoplasmic injected poly I:C also activate endosomal TLR3 and TRIF dependent downstream signaling. As microinjections produce undetectable amount of extracellular poly I:C, the activation of TLR3 must be caused by poly I:C reside in cytosol. Previous studies demonstrated that PKR upon activation promoted SG formation, which subsequently halted mRNA translocation in eukaryotic cells. Therefore, I hypothesized that an inhibitory protein with a short half-life circle links PKR and TLR3 in the cell death induced by poly I:C injection. cFLIP is a CHX sensitive inhibitor of caspase 8 known to regulate TLR3 dependent cell death signal. cFLIP expression level was then examined under CHX treatment or the activation of PKR in HeLa cells. As expected, cFLIP levels significantly decreased after these treatments (Figure. 6A, D). Furthermore, knockdown and overexpression of cFLIP enhanced and attenuated cell death, respectively (Figure. 6E, F), suggesting that cFLIP is a negative regulator of apoptosis firmly targeted by PKR. However, the level of another apoptotic inhibitor cIAP was not shown to be affected by PKR activation (data not shown). Moreover, the expression level of cFLIP was not only regulated by PKR through the protein synthesis arrest, TLR3 also shown time-dependent regulation of cFLIP L and S isoform. At an early stage of TLR3 activation, reduced cFLIP L levels were also detected (3 h) (Figure. 6B, D), consistently a transient loss of cell viability was observed at 3-6 h (Figure. 4E). However, no cell death was markedly induced (Figure. 4E) as further increases of cFLIP S levels during the treatment of poly I:C (Figure. 6B, C, D). According to this finding, the restricted down-regulation of cFLIP induced by TLR3 may be caused by the autocleavage of the cFLIP L/caspase 8 heterodimer with insufficient cell death signals. (Kataoka & Tschopp, 2004; Krueger et al., 2001; Micheau et al., 2002) . These results further emphasized the importance of PKR which controls the apoptotic balance by modulating cFLIP expression. Caspases 8 and 9 are crucial initiator of apoptosis. Selective activation of PKR (by coumermycin A1) and TLR3 (by poly I:C treatment) weakly promoted the cleavage of caspases 8 and 9, respectively, and combined treatment resulted in the remarkable cleavage of these caspases (Figure. 6D). This is consistent with studies of PKR KO, TRIF KO, and DKO HeLa cells under poly I:C transfection (Figure. 6G). Therefore, it suggested that

cytoplasmic dsRNA triggered two pathways regulated by PKR and TLR3, both of which are necessary for the full execution of final apoptosis. CHX dependent inhibition of protein translation exhibit similar effects as PKR activation and further cell death induction (Figure. 6D), suggesting that the main mechanism mediated by PKR is translational arrest. Moreover, overexpression of cFLIP did not completely rescue PKR activation-induced apoptosis (Figure. 6F), suggesting that PKR also triggers cFLIP-independent cell death signal, possibly via the intrinsic mitochondrial pathway. The regulation of cell death via two independent mechanisms is not limited to that induced by dsRNA. TNF-α, which did not induce apoptosis by itself, synergistically induced apoptosis when combined with translational arrest by CHX treatment or PKR activation (Figure. 6I). And this phenomenon is not restricted to HeLa cells, HT1080 cells derived from fibrosarcoma also exhibited similar cell death pattern when stimulated with exogenous poly I:C and CHX (Figure S2B). Since the phosphorylation of eIF2α is catalyzed by multiple stress-induced kinases including PKR, PARK, HRI, and GCN2, cellular stress may be conditional for the induction of apoptosis. However, PKR-regulated signaling did not cooperate with that triggered by RLRs for cell death (Figure. 4G), further confirming that the central function of RLRs is to promote IFN-I and antiviral protein production.

Next the impact of dsRNA-induced cell death on virus production were examined. The results obtained revealed that PKR and TRIF were required for efficient cell death under the infection of SeV and SINV, which are negative- and positive-strand RNA viruses (Figure. 7A, D). Importantly, the viral yield was increased by the inhibition of cell death via the PKR and TRIF deletion or by the Z-VAD treatment (Figure. 7B, C, E, F). PKR and TRIF each played an essential role in the process of anti-viral immunity. PKR blocks viral protein translation and promotes viral RNA recognition by inducing SG (Gal-Ben-Ari et al., 2018; Onomoto et al., 2012), on the other hands, TRIF is necessary for TLR3-dependent IFN-I production and ISG expression (Yamamoto et al., 2003). The present study demonstrated the importance of PKR and TLR3/TRIF from the perspective of cell death induction as well as the resulting inhibitory effects on virus production, it highlighted the role of PKR and translational arrest in cell death induction in the cancer cells. As a conclusion, both antiviral protein production and the robust cell death mediated by PKR and TRIF are important

antiviral signaling triggered by viral dsRNA via distinct pathways in infected cells. Defects in PKR or TRIF resulted in increased viral proliferation and severe infection damage.

Finally, this study further developed the utilization of microinjection, which allows investigations of the stimulatory effects of *in vitro* transcribed nucleic acid products, purified proteins, and their mixtures in single cells. It is worth mentioning that due to its self-restricted structure, RIG-I failed to induce IRF-3 translocation by injection, however, MDA5, which is believed to have an opened structure was found to activation IRF-3 by direct injection, nevertheless, MDA5 G821S mutant that causes autoimmune disorder in mice were found to activate IRF-3 more efficiently than wt MDA5 by cytoplasmic injection (Figure S1B). These results further revealed the potential use of microinjection for the study of protein function.

CHAPTER 5

BIBLIOGRAPHY

BIBLIOGRAPHY

Abe, H., Satoh, J., Shirasaka, Y., Kogure, A., Kato, H., Ito, S., & Fujita, T. (2020). Priming Phosphorylation of TANK-Binding Kinase 1 by IκB Kinase β Is Essential in Toll-Like Receptor 3/4 Signaling. *Molecular and Cellular Biology*, *40*(5). https://doi.org/10.1128/MCB.00509-19

Akira, S., Takeda, K., & Kaisho, T. (2001). Toll-like receptors: critical proteins linking innate and acquired immunity. *Nature Immunology*, *2*(8), 675–680. https://doi.org/10.1038/90609

Alkurdi, L., Virard, F., Vanbervliet, B., Weber, K., Toscano, F., Bonnin, M., le Stang, N., Lantuejoul, S., Micheau, O., Renno, T., Lebecque, S., & Estornes, Y. (2018). Release of c-FLIP brake selectively sensitizes human cancer cells to TLR3-mediated apoptosis. *Cell Death and Disease*, *9*(9). https://doi.org/10.1038/s41419-018-0850-0

Bergsbaken, T., Fink, S. L., & Cookson, B. T. (2009). Pyroptosis: host cell death and inflammation. *Nature Reviews. Microbiology*, *7*(2), 99–109. https://doi.org/10.1038/nrmicro2070

Boehmer, D. F. R., Formisano, S., de Oliveira Mann, C. C., Mueller, S. A., Kluge, M., Metzger, P., Rohlfs, M., Hörth, C., Kocheise, L., Lichtenthaler, S. F., Hopfner, K. P., Endres, S., Rothenfusser, S., Friedel, C. C., Duewell, P., Schnurr, M., & Koenig, L. M. (2021). OAS1/RNase L executes RIG-I ligand–dependent tumor cell apoptosis. *Science Immunology*, *6*(61). https://doi.org/10.1126/sciimmunol.abe2550

Bürckstümmer, T., Baumann, C., Blüml, S., Dixit, E., Dürnberger, G., Jahn, H., Planyavsky, M., Bilban, M., Colinge, J., Bennett, K. L., & Superti-Furga, G. (2009). An orthogonal proteomic-genomic screen identifies AIM2 as a cytoplasmic DNA sensor for the inflammasome. *Nature Immunology*, *10*(3), 266–272. https://doi.org/10.1038/ni.1702

Chattopadhyay, S., Kuzmanovic, T., Zhang, Y., Wetzel, J. L., & Sen, G. C. (2016). Ubiquitination of the Transcription Factor IRF-3 Activates RIPA, the Apoptotic Pathway that Protects Mice from Viral Pathogenesis. *Immunity*, *44*(5), 1151–1161. https://doi.org/10.1016/j.immuni.2016.04.009

Donovan, J., Dufner, M., & Korennykh, A. (2013). Structural basis for cytosolic double-stranded RNA surveillance by human oligoadenylate synthetase 1. *Proceedings of the National*

Academy of Sciences of the United States of America, *110*(5), 1652–1657. https://doi.org/10.1073/pnas.1218528110

Duic, I., Tadakuma, H., Harada, Y., Yamaue, R., Deguchi, K., Suzuki, Y., Yoshimura, S. H., Kato, H., Takeyasu, K., & Fujita, T. (2020). Viral RNA recognition by LGP2 and MDA5, and activation of signaling through step-by-step conformational changes. *Nucleic Acids Research*, *48*(20), 11664–11674. https://doi.org/10.1093/nar/gkaa935

Elmore, S. (2007). Apoptosis: a review of programmed cell death. *Toxicologic Pathology*, *35*(4), 495–516. https://doi.org/10.1080/01926230701320337

Fitzgerald, K. A., McWhirter, S. M., Faia, K. L., Rowe, D. C., Latz, E., Golenbock, D. T., Coyle, A. J., Liao, S.-M., & Maniatis, T. (2003). IKKepsilon and TBK1 are essential components of the IRF3 signaling pathway. *Nature Immunology*, *4*(5), 491–496. https://doi.org/10.1038/ni921

Franchi, L., Eigenbrod, T., Muñoz-Planillo, R., Ozkurede, U., Kim, Y.-G., Arindam, C., Gale, M., Silverman, R. H., Colonna, M., Akira, S., & Núñez, G. (2014). Cytosolic double-stranded RNA activates the NLRP3 inflammasome via MAVS-induced membrane permeabilization and K+ efflux. *Journal of Immunology (Baltimore, Md. : 1950)*, *193*(8), 4214–4222. https://doi.org/10.4049/jimmunol.1400582

Friedrich, I., Eizenbach, M., Sajman, J., Ben-Bassat, H., & Levitzki, A. (2005). A cellular screening assay to test the ability of PKR to induce cell death in mammalian cells. *Molecular Therapy*, *12*(5), 969–975. https://doi.org/10.1016/j.ymthe.2005.06.442

Fritsch, M., Günther, S. D., Schwarzer, R., Albert, M.-C., Schorn, F., Werthenbach, J. P., Schiffmann, L. M., Stair, N., Stocks, H., Seeger, J. M., Lamkanfi, M., Krönke, M., Pasparakis, M., & Kashkar, H. (2019). Caspase-8 is the molecular switch for apoptosis, necroptosis and pyroptosis. *Nature*, *575*(7784), 683–687. https://doi.org/10.1038/s41586-019-1770-6

Gal-Ben-Ari, S., Barrera, I., Ehrlich, M., & Rosenblum, K. (2018). PKR: A Kinase to Remember. *Frontiers in Molecular Neuroscience*, *11*, 480. https://doi.org/10.3389/fnmol.2018.00480

García, M. A., Meurs, E. F., & Esteban, M. (2007). The dsRNA protein kinase PKR: virus and cell control. *Biochimie*, *89*(6–7), 799–811. https://doi.org/10.1016/j.biochi.2007.03.001

Geserick, P., Drewniok, C., Hupe, M., Haas, T. L., Diessenbacher, P., Sprick, M. R., Schön, M. P.,

Henkler, F., Gollnick, H., Walczak, H., & Leverkus, M. (2008). Suppression of cFLIP is sufficient to sensitize human melanoma cells to TRAIL- and CD95L-mediated apoptosis. *Oncogene*, *27*(22), 3211–3220. https://doi.org/10.1038/sj.onc.1210985

Gil, J., & Esteban, M. (2000). The interferon-induced protein kinase (PKR), triggers apoptosis through FADD-mediated activation of caspase 8 in a manner independent of Fas and TNF-α receptors. *Oncogene*, *19*(32), 3665–3674. https://doi.org/10.1038/sj.onc.1203710

Gil, J., García, M. A., & Esteban, M. (2002). Caspase 9 activation by the dsRNA-dependent protein kinase, PKR: molecular mechanism and relevance. *FEBS Letters*, *529*(2–3), 249–255. https://doi.org/10.1016/s0014-5793(02)03348-3

Han, Y., Donovan, J., Rath, S., Whitney, G., Chitrakar, A., & Korennykh, A. (2014). Structure of human RNase L reveals the basis for regulated RNA decay in the IFN response. *Science (New York, N.Y.)*, *343*(6176), 1244–1248. https://doi.org/10.1126/science.1249845

Hart, P. D., & Young, M. R. (1991). Ammonium chloride, an inhibitor of phagosome-lysosome fusion in macrophages, concurrently induces phagosome-endosome fusion, and opens a novel pathway: studies of a pathogenic mycobacterium and a nonpathogenic yeast. *The Journal of Experimental Medicine*, *174*(4), 881–889. https://doi.org/10.1084/jem.174.4.881

Hornung, V., Ellegast, J., Kim, S., Brzózka, K., Jung, A., Kato, H., Poeck, H., Akira, S., Conzelmann, K. K., Schlee, M., Endres, S., & Hartmann, G. (2006). 5′-Triphosphate RNA is the ligand for RIG-I. *Science*, *314*(5801), 994–997. https://doi.org/10.1126/science.1132505

Hou, F., Sun, L., Zheng, H., Skaug, B., Jiang, Q.-X., & Chen, Z. J. (2011a). *MAVS Forms Functional Prion-Like Aggregates To Activate and Propagate Antiviral Innate Immune Response*. https://doi.org/10.1016/j.cell.2011.06.041

Hsu, L. C., Park, J. M., Zhang, K., Luo, J. L., Maeda, S., Kaufman, R. J., Eckmann, L., Guiney, D. G., & Karin, M. (2004). The protein kinase PKR is required for macrophage apoptosis after activation of Toll-like receptor 4. *Nature*, *428*(6980), 341–345. https://doi.org/10.1038/nature02405

Hu, S., Sun, H., Yin, L., Li, J., Mei, S., Xu, F., Wu, C., Liu, X., Zhao, F., Zhang, D., Huang, Y., Ren, L., Cen, S., Wang, J., Liang, C., & Guo, F. (2019). PKR-dependent cytosolic cGAS foci are necessary for intracellular DNA sensing. *Science Signaling*, *12*(609).

https://doi.org/10.1126/scisignal.aav7934

Jagus, R., Joshi, B., & Barber, G. N. (1999). PKR, apoptosis and cancer. *International Journal of Biochemistry and Cell Biology*, *31*(1), 123–138. https://doi.org/10.1016/S1357-2725(98)00136-8

Janeway, C. A., & Medzhitov, R. (2002). Innate immune recognition. *Annual Review of Immunology*, *20*, 197–216. https://doi.org/10.1146/annurev.immunol.20.083001.084359

Kasumba, D. M., Hajake, T., Oh, S.-W., Kotenko, S. v, Kato, H., & Fujita, T. (2017). A Plant-Derived Nucleic Acid Reconciles Type I IFN and a Pyroptotic-like Event in Immunity against Respiratory Viruses. *Journal of Immunology (Baltimore, Md. : 1950)*, *199*(7), 2460–2474. https://doi.org/10.4049/jimmunol.1700523

Kataoka, T., & Tschopp, J. (2004). N-Terminal Fragment of c-FLIP(L) Processed by Caspase 8 Specifically Interacts with TRAF2 and Induces Activation of the NF-κB Signaling Pathway. *Molecular and Cellular Biology*, *24*(7), 2627–2636. https://doi.org/10.1128/MCB.24.7.2627-2636.2004

Kato, H., Oh, S.-W., & Fujita, T. (2017). RIG-I-Like Receptors and Type I Interferonopathies. *Journal of Interferon & Cytokine Research : The Official Journal of the International Society for Interferon and Cytokine Research*, *37*(5), 207–213. https://doi.org/10.1089/jir.2016.0095

Kato, H., Takeuchi, O., Mikamo-Satoh, E., Hirai, R., Kawai, T., Matsushita, K., Hiiragi, A., Dermody, T. S., Fujita, T., & Akira, S. (2008). Length-dependent recognition of double-stranded ribonucleic acids by retinoic acid-inducible gene-I and melanoma differentiation-associated gene 5. *The Journal of Experimental Medicine*, *205*(7), 1601–1610. https://doi.org/10.1084/jem.20080091

Kato, H., Takeuchi, O., Sato, S., Yoneyama, M., Yamamoto, M., Matsui, K., Uematsu, S., Jung, A., Kawai, T., Ishii, K. J., Yamaguchi, O., Otsu, K., Tsujimura, T., Koh, C.-S., Reis e Sousa, C., Matsuura, Y., Fujita, T., & Akira, S. (2006). Differential roles of MDA5 and RIG-I helicases in the recognition of RNA viruses. *Nature*, *441*(7089), 101–105. https://doi.org/10.1038/nature04734

Kawai, T., & Akira, S. (2006). Innate immune recognition of viral infection. *Nature Immunology*, *7*(2), 131–137. https://doi.org/10.1038/ni1303

Kawai, T., & Akira, S. (2010). The role of pattern-recognition receptors in innate immunity: update on Toll-like receptors. *Nature Immunology*, *11*(5), 373–384. https://doi.org/10.1038/ni.1863

Kawai, T., Takahashi, K., Sato, S., Coban, C., Kumar, H., Kato, H., Ishii, K. J., Takeuchi, O., & Akira, S. (2005). IPS-1, an adaptor triggering RIG-I- and Mda5-mediated type I interferon induction. *Nature Immunology*, *6*(10), 981–988. https://doi.org/10.1038/ni1243

Kreuz, S., Siegmund, D., Scheurich, P., & Wajant, H. (2001). NF-kappaB inducers upregulate cFLIP, a cycloheximide-sensitive inhibitor of death receptor signaling. *Molecular and Cellular Biology*, *21*(12), 3964–3973. https://doi.org/10.1128/MCB.21.12.3964-3973.2001

Krueger, A., Schmitz, I., Baumann, S., Krammer, P. H., & Kirchhoff, S. (2001). Cellular FLICE-inhibitory protein splice variants inhibit different steps of caspase-8 activation at the CD95 death-inducing signaling complex. *The Journal of Biological Chemistry*, *276*(23), 20633–20640. https://doi.org/10.1074/jbc.M101780200

Kuznik, A., Bencina, M., Svajger, U., Jeras, M., Rozman, B., & Jerala, R. (2011). Mechanism of endosomal TLR inhibition by antimalarial drugs and imidazoquinolines. *Journal of Immunology (Baltimore, Md. : 1950)*, *186*(8), 4794–4804. https://doi.org/10.4049/jimmunol.1000702

Lei, Y., Moore, C. B., Liesman, R. M., O'Connor, B. P., Bergstralh, D. T., Chen, Z. J., Pickles, R. J., & Ting, J. P.-Y. (2009). MAVS-mediated apoptosis and its inhibition by viral proteins. *PloS One*, *4*(5), e5466. https://doi.org/10.1371/journal.pone.0005466

Lemaire, P. A., Anderson, E., Lary, J., & Cole, J. L. (2008). Mechanism of PKR Activation by dsRNA. *Journal of Molecular Biology*, *381*(2), 351–360. https://doi.org/10.1016/j.jmb.2008.05.056

Li, J., Cao, F., Yin, H.-L., Huang, Z.-J., Lin, Z.-T., Mao, N., Sun, B., & Wang, G. (2020). Ferroptosis: past, present and future. *Cell Death & Disease*, *11*(2), 88. https://doi.org/10.1038/s41419-020-2298-2

Liddicoat, B. J., Piskol, R., Chalk, A. M., Ramaswami, G., Higuchi, M., Hartner, J. C., Li, J. B., Seeburg, P. H., & Walkley, C. R. (2015). RNA editing by ADAR1 prevents MDA5 sensing of endogenous dsRNA as nonself. *Science*, *349*(6252), 1115–1120. https://doi.org/10.1126/science.aac7049

McAllister, C. S., Lakhdari, O., Chambrun, G. P. de, Gareau, M. G., Broquet, A., Lee, G. H., Shenouda, S., Eckmann, L., & Kagnoff, M. F. (2013). TLR3, TRIF and Caspase 8 determine double-stranded RNA-induced epithelial cell death and survival in vivo. *Journal of Immunology (Baltimore, Md. : 1950)*, *190*(1), 418. https://doi.org/10.4049/JIMMUNOL.1202756

Medzhitov, R., Preston-Hurlburt, P., Kopp, E., Stadlen, A., Chen, C., Ghosh, S., & Janeway, C. A. (1998). MyD88 is an adaptor protein in the hToll/IL-1 receptor family signaling pathways. *Molecular Cell*, *2*(2), 253–258. https://doi.org/10.1016/s1097-2765(00)80136-7

Micheau, O., Thome, M., Schneider, P., Holler, N., Tschopp, J., Nicholson, D. W., Briand, C., & Grütter, M. G. (2002). The long form of FLIP is an activator of caspase-8 at the Fas death-inducing signaling complex. *The Journal of Biological Chemistry*, *277*(47), 45162–45171. https://doi.org/10.1074/jbc.M206882200

Mizushima, S., & Nagata, S. (1990). pEF-BOS, a powerful mammalian expression vector. *Nucleic Acids Research*, *18*(17), 5322. https://doi.org/10.1093/nar/18.17.5322

Moody, S. A. (2018). Microinjection of mRNAs and Oligonucleotides. *Cold Spring Harbor Protocols*, *2018*(12). https://doi.org/10.1101/pdb.prot097261

Onomoto, K., Jogi, M., Yoo, J. S., Narita, R., Morimoto, S., Takemura, A., Sambhara, S., Kawaguchi, A., Osari, S., Nagata, K., Matsumiya, T., Namiki, H., Yoneyama, M., & Fujita, T. (2012). Critical role of an antiviral stress granule containing RIG-I and PKR in viral detection and innate immunity. *PLoS ONE*, *7*(8). https://doi.org/10.1371/journal.pone.0043031

Oshiumi, H., Matsumoto, M., Funami, K., Akazawa, T., & Seya, T. (2003). TICAM-1, an adaptor molecule that participates in Toll-like receptor 3-mediated interferon-β induction. *Nature Immunology*, *4*(2), 161–167. https://doi.org/10.1038/ni886

Pichlmair, A., Schulz, O., Tan, C. P., Näslund, T. I., Liljeström, P., Weber, F., & Reis e Sousa, C. (2006). RIG-I-mediated antiviral responses to single-stranded RNA bearing 5'-phosphates. *Science (New York, N.Y.)*, *314*(5801), 997–1001. https://doi.org/10.1126/science.1132998

Raja, R., & Sen, G. C. (2021). The antiviral action of the RIG-I induced pathway of apoptosis (RIPA) is enhanced by its ability to degrade Otulin, which deubiquitinates IRF3. *Cell Death and Differentiation*. https://doi.org/10.1038/s41418-021-00870-4

Renauld, J.-C. (2003). Class II cytokine receptors and their ligands: key antiviral and inflammatory modulators. *Nature Reviews. Immunology*, *3*(8), 667–676. https://doi.org/10.1038/nri1153

Safa, A. R. (2012). c-FLIP, a master anti-apoptotic regulator. *Experimental Oncology*, *34*(3), 176–184.

Saito, T., Hirai, R., Loo, Y.-M., Owen, D., Johnson, C. L., Sinha, S. C., Akira, S., Fujita, T., & Gale, M. (2007). Regulation of innate antiviral defenses through a shared repressor domain in RIG-I and LGP2. *Proceedings of the National Academy of Sciences of the United States of America*, *104*(2), 582–587. https://doi.org/10.1073/pnas.0606699104

Salaun, B., Coste, I., Rissoan, M.-C., Lebecque, S. J., & Renno, T. (2006). TLR3 Can Directly Trigger Apoptosis in Human Cancer Cells. *The Journal of Immunology*, *176*(8), 4894–4901. https://doi.org/10.4049/jimmunol.176.8.4894

Samuel, C. E. (1993). The eIF-2 alpha protein kinases, regulators of translation in eukaryotes from yeasts to humans. *The Journal of Biological Chemistry*, *268*(11), 7603–7606.

Satoh, T., Kato, H., Kumagai, Y., Yoneyama, M., Sato, S., Matsushita, K., Tsujimura, T., Fujita, T., Akira, S., & Takeuchi, O. (2010). LGP2 is a positive regulator of RIG-I- and MDA5-mediated antiviral responses. *Proceedings of the National Academy of Sciences of the United States of America*, *107*(4), 1512–1517. https://doi.org/10.1073/pnas.0912986107

Seth, R. B., Sun, L., Ea, C. K., & Chen, Z. J. (2005). Identification and Characterization of MAVS, a Mitochondrial Antiviral Signaling Protein that Activates NF-κB and IRF3. *Cell*, *122*(5), 669–682. https://doi.org/10.1016/J.CELL.2005.08.012

Sun, L., Wu, J., Du, F., Chen, X., & Chen, Z. J. (2013). Cyclic GMP-AMP synthase is a cytosolic DNA sensor that activates the type I interferon pathway. *Science (New York, N.Y.)*, *339*(6121), 786–791. https://doi.org/10.1126/science.1232458

Swanson, K. v., Deng, M., & Ting, J. P.-Y. (2019). The NLRP3 inflammasome: molecular activation and regulation to therapeutics. *Nature Reviews Immunology*, *19*(8), 477–489. https://doi.org/10.1038/s41577-019-0165-0

Takahasi, K., Onomoto, K., Horiuchi, M., Kato, H., Fujita, T., & Yoneyama, M. (2019). Identification of a new autoinhibitory domain of interferon-beta promoter stimulator-1 (IPS-1) for the tight regulation of oligomerization-driven signal activation. *Biochemical and*

Biophysical Research Communications, *517*(4), 662–669. https://doi.org/10.1016/j.bbrc.2019.07.099

Takahasi, K., Yoneyama, M., Nishihori, T., Hirai, R., Kumeta, H., Narita, R., Gale, M., Inagaki, F., & Fujita, T. (2008). Nonself RNA-sensing mechanism of RIG-I helicase and activation of antiviral immune responses. *Molecular Cell*, *29*(4), 428–440. https://doi.org/10.1016/j.molcel.2007.11.028

Takamatsu, S., Onoguchi, K., Onomoto, K., Narita, R., Takahasi, K., Ishidate, F., Fujiwara, T. K., Yoneyama, M., Kato, H., & Fujita, T. (2013). Functional characterization of domains of IPS-1 using an inducible oligomerization system. *PloS One*, *8*(1), e53578. https://doi.org/10.1371/journal.pone.0053578

Tiefenboeck, P., Kim, J. A., & Leroux, J.-C. (2018). Intracellular delivery of colloids: Past and future contributions from microinjection. *Advanced Drug Delivery Reviews*, *132*, 3–15. https://doi.org/10.1016/j.addr.2018.06.013

Tsuchiya, Y., Nakabayashi, O., & Nakano, H. (2015). FLIP the switch: Regulation of apoptosis and necroptosis by cFLIP. *International Journal of Molecular Sciences*, *16*(12), 30321–30341. https://doi.org/10.3390/ijms161226232

Ung, T. L., Cao, C., Lu, J., Ozato, K., & Dever, T. E. (2001). Heterologous dimerization domains functionally substitute for the double-stranded RNA binding domains of the kinase PKR. *The EMBO Journal*, *20*(14), 3728–3737. https://doi.org/10.1093/emboj/20.14.3728

Vandenabeele, P., Galluzzi, L., vanden Berghe, T., & Kroemer, G. (2010). Molecular mechanisms of necroptosis: an ordered cellular explosion. *Nature Reviews. Molecular Cell Biology*, *11*(10), 700–714. https://doi.org/10.1038/nrm2970

Xu, W. (2019). Microinjection and Micromanipulation: A Historical Perspective. *Methods in Molecular Biology (Clifton, N.J.)*, *1874*, 1–16. https://doi.org/10.1007/978-1-4939-8831-0_1

Yamamoto, M., Sato, S., Hemmi, H., Hoshino, K., Kaisho, T., Sanjo, H., Takeuchi, O., Sugiyama, M., Okabe, M., Takeda, K., & Akira, S. (2003). Role of adaptor TRIF in the MyD88-independent toll-like receptor signaling pathway. *Science*, *301*(5633), 640–643. https://doi.org/10.1126/science.1087262

Yeung, M. C., Liu, J., & Lau, A. S. (1996). An essential role for the interferon-inducible,

double-stranded RNA-activated protein kinase PKR in the tumor necrosis factor-induced apoptosis in U937 cells. *Proceedings of the National Academy of Sciences of the United States of America*, *93*(22), 12451–12455. https://doi.org/10.1073/pnas.93.22.12451

Yoneyama, M., & Fujita, T. (2008). Structural Mechanism of RNA Recognition by the RIG-I-like Receptors. *Immunity*, *29*(2), 178–181. https://doi.org/10.1016/j.immuni.2008.07.009

Yoneyama, M., Kikuchi, M., Matsumoto, K., Imaizumi, T., Miyagishi, M., Taira, K., Foy, E., Loo, Y.-M., Gale, M., Akira, S., Yonehara, S., Kato, A., & Fujita, T. (2005). Shared and Unique Functions of the DExD/H-Box Helicases RIG-I, MDA5, and LGP2 in Antiviral Innate Immunity. *The Journal of Immunology*, *175*(5), 2851–2858. https://doi.org/10.4049/jimmunol.175.5.2851

Yoneyama, M., Kikuchi, M., Natsukawa, T., Shinobu, N., Imaizumi, T., Miyagishi, M., Taira, K., Akira, S., & Fujita, T. (2004). The RNA helicase RIG-I has an essential function in double-stranded RNA-induced innate antiviral responses. *Nature Immunology*, *5*(7), 730–737. https://doi.org/10.1038/ni1087

Yoneyama, M., Suhara, W., Fukuhara, Y., Fukuda, M., Nishida, E., & Fujita, T. (1998a). Direct triggering of the type I interferon system by virus infection: Activation of a transcription factor complex containing IRF-3 and CBP/p300. *EMBO Journal*, *17*(4), 1087–1095.

CHAPTER 6

ACKNOWLEDGEMENT

ACKNOWLEDGEMENT

This thesis is based on the material contained in the following scholarly paper:

PKR and TLR3 trigger distinct signals that coordinate the induction of antiviral apoptosis

Wenjie Zuo, Mai Wakimoto, Noriyasu Kozaiwa, Yutaro Shirasaka, Seong-Wook Oh, Shiori Fujiwara, Hitoshi. Miyachi, Amane Kogure, Hiroki Kato, Takashi Fujita